Spring 2014

Investigation of angiogenic effects of bioactive borate glass microfibers and beads in a rodent model

Richard Jeffrey Watters

Department:

INVESTIGATION OF ANGIOGENIC EFFECTS OF BIOACTIVE BORATE GLASS MICROFIBERS AND BEADS IN A RODENT MODEL

By

RICHARD JEFFREY WATTERS

A THESIS

Presented to the Faculty of the Graduate School of the

MISSOURI UNIVERSITY OF SCIENCE AND TECHNOLOGY

In Partial Fulfillment of the Requirements for the Degree

MASTER OF SCIENCE IN APPLIED AND ENVIRONMENTAL BIOLOGY

2014

Approved by

Roger F. Brown, Advisor
Delbert E. Day
Mohamed N. Rahaman

PUBLICATION THESIS OPTION

This thesis has been prepared in the style used for publication in the peer reviewed journal by the *Journal of Biomedical Materials Research*. Pages 1 through 63 are intended to be submitted for publication in that journal.

ABSTRACT

The primary objective of this research project was to evaluate the effects of three different compositions of bioactive glass microfibers (45S5, 13-93B3, and 13-93B3Cu) and bioactive glass beads (13-93, 13-93B3, and 13-93B3Cu) on angiogenesis in subcutaneous tissue in the SKH1 'hairless' mouse. Microvascular responses to the bioactive glass implants were investigated via three experimental approaches: noninvasive vital imaging of microvasculature in dorsal skin windows; quantitative histomorphometry of microvascular densities; and quantitative PCR measurements of mRNA expression of pro-angiogenic cytokines VEGF and FGF-2. The live imaging of dorsal skin window preparations in the hairless SKH1 showed the formation of a halo-like structure infused with vessels in soft tissue surrounding borate-based 13-93B3 and 13-93B3Cu glass beads two weeks after implantation. This response was not observed around silicate-based 13-93 glass beads. Quantitative histomorphometry of tissue implanted with 45S5, 13-93B3, and 13-93B3Cu glass microfiber plugs revealed microvascular densities that were 1.6-, 2.3-, and 2.7-fold higher, respectively compared to the sham control tissues whereas the 13-93, 13-93B3, and 13-93B3Cu glass beads produced a 1.3-, 1.6-, and 2.5-fold increase, respectively, compared to the sham control. Quantitative PCR measurements indicate a marginally significant increase in expression of VEGF mRNA in skin tissues with 13-93B3Cu. This latter outcome supports the project hypothesis that 13-93B3Cu glass induces VEGF expression followed by neovascularization, a key process of wound healing.

ACKNOWLEDGEMENTS

This thesis would not have been possible without the help and guidance of several individuals. These individuals contributed greatly to the completion of this study.

I would first like to thank my advisor, Dr. Roger Brown, for the opportunity to complete this study. His time, effort, wisdom, and patience were always greatly appreciated and his exceptional guidance throughout this thesis was instrumental. I would like to thank Dr. Delbert E. Day and Dr. Rahaman for their encouragement and contributions towards this project. I offer a special thanks to Dr. Robert Aronstam, the Chairman of the Biological Sciences department for the helpful discussions, comments, and suggestions throughout my education. I would also like to thank the Mo-Sci Corporation for the bioactive glass materials used in this study and the Center for Biomedical Science and Engineering.

All of my friends deserve special thanks as well. I am thankful for Yinan Lin, a good friend, who taught many of the procedures used in this study and Ali Mohammadkhah for helping collect samples from the field. My research would not have been possible without their help.

Last but not the least; I cannot say enough about the support I have received from both my parents, Chris and Lori Watters. They were always there encouraging me to succeed throughout this entire project and their support always helped me when I needed it most. Thank you.

TABLE OF CONTENTS

Page

LIST OF ILLUSTRATIONS

Page

LIST OF TABLES

Page

PAPER

In Vivo Evaluation of Angiogenic Effects of Borate Glass in the SKH1 Hairless Mouse

Richard Watters, Roger F. Brown[a1], Delbert E. Day[b]

Departments of Biological Sciences[a] and Materials Science and Engineering[b]

Missouri University of Science and Technology, Rolla, MO 65409-1120

[1]Corresponding Author. Fax: (573)341-4860; email:rbrown@mst.edu

ABSTRACT

The primary objective of this research project was to evaluate the effects of three different compositions of bioactive glass microfibers (45S5, 13-93B3, and 13-93B3Cu) and bioactive glass beads (13-93, 13-93B3, and 13-93B3Cu) on angiogenesis in subcutaneous tissue in the SKH1 'hairless' mouse. Microvascular responses to the bioactive glass implants were investigated via three experimental approaches: noninvasive vital imaging of microvasculature in dorsal skin windows; quantitative histomorphometry of microvascular densities; and quantitative PCR measurements of mRNA expression of pro-angiogenic cytokines VEGF and FGF-2. The live imaging of dorsal skin window preparations in the hairless SKH1 showed the formation of a halo-like structure infused with vessels in soft tissue surrounding borate-based 13-93B3 and 13-93B3Cu glass beads two weeks after implantation. This response was not observed around silicate-based 13-93 glass beads. Quantitative histomorphometry of tissue implanted with 45S5, 13-93B3, and 13-93B3Cu glass microfiber plugs revealed microvascular densities that were 1.6-, 2.3-, and 2.7-fold higher, respectively compared to the sham control tissues whereas the 13-93, 13-93B3, and 13-93B3Cu glass beads produced a 1.3-, 1.6-, and 2.5-fold increase, respectively, compared to the sham control. Quantitative PCR measurements indicate a marginally significant increase in expression of VEGF mRNA in skin tissues with 13-93B3Cu. This latter outcome supports the project hypothesis that 13-93B3Cu glass induces VEGF expression followed by neovascularization, a key process of wound healing.

I. INTRODUCTION

Each year approximately 6.5 million people in the United States receive treatment for non-healing chronic skin wounds. This is a significant health care problem that costs an estimated $25 billion dollars annually [1]. Chronic skin wounds are wounds that do not heal within three months and consist of three primary types: venous ulcers, diabetic ulcers, and pressure ulcers [2]. Chronic wounds frequently become infected and gangrenous, often resulting in amputation and dramatically higher mortality rates [3]. Diabetic ulcers of the foot present a special challenge due to the characteristically diminished blood flow of diabetic patients, a characteristic that impedes the healing of soft tissue wounds [4].

Wound healing consists of three overlapping phases which include inflammation, proliferation, and maturation [5-7]. The inflammatory phase begins with hemostasis. This halts the ongoing loss of blood and fluid loss, and continues with release of cytokines that make the wound hypoxic, thus creating an environment that recruits T cells [8-9]. The proliferation phase includes the release of specific growth factors that trigger the formation of granulation tissue. The newly formed blood vessels of this tissue are responsible for its reddish, granular appearance which is the basis of the tissue name. The maturation phase includes the remodeling and realignment of collagen fibers along lines of tension, creating an increase in tensile strength of wound tissue. The full cause of impaired wound healing in chronic soft tissue wounds remains uncertain despite extensive research.

Neovascularization or angiogenesis plays a crucial role in the healing of soft tissue wounds. The importance of this process is emphasized by the discovery that

insufficient angiogenesis is a hallmark of chronic wound healing as seen in diabetic patients with chronic venous stasis wounds [10-17]. The finding that specific angiogenic cytokines are often absent or deficient in patients with chronic wounds has prompted the use of various pro-angiogenic growth factors in clinical trials for the treatment of chronic wounds [18]. The pro-angiogenic growth factor platelet derived growth factor (PDGF) is the active component of a topical gel (Becaplermin) for the treatment of lower extremity ulcers [19]. Other experimental trials with positive results have involved the use of vascular endothelial growth factor A (VEGFA) and fibroblast growth factor B (bFGF or FGF2), two of the known positive regulators of angiogenesis [20,21]. Currently, PDGF remains the only growth factor approved by the FDA for treating non-healing chronic wounds in humans [22].

The standard procedures currently used to treat and manage skin wounds include the administration of antibiotics, debridement of necrotic tissue with repeat applications of wound dressings, compression therapy, plus various nutritional supplements [23-26]. These conventional procedures often demonstrate limited efficacy in the treatment chronic wounds. This limited effectiveness has prompted use of more aggressive treatment options such as negative pressure treatments [27], hyperbaric chambers [28], oxygen therapy [29], and the transplantation of cultured human dermis [30,31]. Although these more aggressive treatments have had limited success, they have a minimal impact due to their limited availability, excessively high cost, and other factors.

A new, simpler, and less expensive approach to cytokine-induced angiogenesis is the incorporation of pro-angiogenic ions in wound treatment materials. A number of ions including copper, cobalt, boron, zinc, and others have been shown to have a physiological

role in angiogenesis [32,33]. Using dissolvable materials containing one or more of these pro-angiogenic ions could be effective for localized delivery of angiogenic ions. Borate-based bioactive glass was recently tested as a delivery device for angiogenic ions in soft tissue repair [34]. Bioactive glass scaffolds doped with copper and other elements were subcutaneously implanted into laboratory rats and left for six weeks. Analysis of tissues implanted with scaffolds prepared from a borate-based glass designated 13-93B3 and 13-93B3 with 0.4% CuO showed a higher density of microvasculature than those with silica-based glass fiber scaffolds [34]. There were however, no sham control tissues included for baseline comparison in that study.

Based on the promising outcome of the murine model, an initial clinical evaluation of the use of borate glass microfibers in wound healing was recently performed by the wound care unit at Phelps County Regional Medical Center (PCRMC). That study included 12 volunteers with chronic venous stasis wounds that were treated topically with repeat microfibrous dressings of 13-93B3 or 13-93B3Cu glass microfibers. The treatments with both glasses were found to help accelerate the healing of previously unresponsive dermal wounds. The chronic wounds were completely healed in 8 out of 12 patients in the clinical study. The clinical staff noticed during daily observations that the 13-93B3 glass appeared to promote re-epithelialization while 13-93B3Cu microfibers appeared to promote granulation in wound healing [35].

A follow up quantitative evaluation of the response of soft tissue to implants of borate-based microfibrous glass was recently conducted in a rodent model [36]. Compressed mats of microfibrous glass were subcutaneously implanted in Sprague Dawley rats and histologically evaluated at two, three, and four week intervals. The

istomorphometric results obtained indicated that borate-based microfibrous glass doped with copper did effectively stimulate angiogenesis.

This study was undertaken to investigate the underlying mechanism of the angiogenic effect of bioactive borate glass. The study involved use of the SKH1 ‘hairless’ mouse with research objective at three distinct biological levels including the macroscopic, tissue, and molecular levels. The macroscopic objective involved real-time imaging of localized tissue responses to bioactive glass using transilluminated dorsal skin fold windows. The second objective was a histomorphometric analysis to quantify the microvascular response to bioactive borate glass in subdermal tissue excised from the dorsum of the mouse. The third objective of this project involved measuring cytokine expression in tissues in response to implantation of copper doped borate glass. The basic hypothesis of this study is that 13-93B3Cu bioactive glass will stimulate expression of the cytokine VEGF resulting in angiogenesis in the treated tissue.

II. MATERIALS AND METHODS

2.1 Experimental design

The experimental design of this project included experiments at three biological levels (macroscopic, tissue, and molecular) to assess the microvascular response to bioactive glass implants in a mouse model system. Two of the three experiments each included ten mice with each animal receiving two subdermal implantations. The surgical implantations in the first experiment included three different types of bioactive glass beads plus the surgery without implantation (sham control). The second experiment involved implantation of three types of glass microfibers plus sham control implantations. The placement of implants was randomized with five replicates of each glass type and five sham controls included in both of the first two experiments. Live transdermal imaging of skin tissues with implants in place was performed at weekly intervals to assess macroscopic responses to the implants. After three weeks, tissues were removed from the implant sites for histological assessment of tissue responses. The third and final experiment included a separate group of eight female mice that were used for assessment of molecular responses to the implants. Each animal received two subdermal implantations followed by re-anesthetization one week later to receive two additional implantations and then, after another week, two additional implantations. There were six total implantations per animal that included three 13-93B3Cu beads and three sham implantations. At 1, 2, and 3 weeks post implantation these animals were euthanized and tissues collected from the implant sites for isolation of total RNA which was used for assay of gene expression.

2.2 Bioactive glass composition and preparation

The bioactive glass materials utilized for subdermal implantation included two types of silica-based glass, 45S5 glass and 13-93 glass, plus two borate-based glasses that were designated 13-93B3 and 13-93B3Cu, all of which were provided by MO-SCI Inc, Rolla, MO. Compositions of these four glasses are listed in Table I. The glass types were used in two physical forms for implantation, plugs of compressed glass microfibers and fused glass beads. Examples of these two types of implants are shown in Figure 1. Batched glass microfibers (10.5 ± 0.5 mg) were compressed into the shape of 2 mm diameter plugs using a specially constructed teflon mold with stainless steel rod inserts. Each compressed plug was displaced from the teflon mold into a 200 µl glass microdispenser tube (Drummond Scientific Company). As shown in Figure 1, the compressed plugs are noticeably porous. The compressed glass microfiber plugs in glass microdispenser tubes were sterilized by dry heating overnight at 300^{o} C prior to implantation. Bioactive glass beads were formed from the glass microfibers using a butane torch (Benzomatic) and a graphite mold. Individual 10 mg ± 0.5 mg batches of the glass microfibers were placed in the graphite mold and heated with the butane torch to fuse the microfibers together to create a smooth spherical body. The individual beads formed were weighed to confirm a mass of 10 mg ± 0.5 mg, checked under a stereoscopic microscope to confirm smoothness plus absence of crystallization, and then dry heat sterilized.

2.3 Dorsal window frame

Special dorsal skin window frames were fabricated from 0.45 mm thick aluminum stock. Individual pieces of the aluminum stock were cut to dimensions of 25 mm x 15

mm with two adjoining pieces used to form one frame. Two windows were bored in each frame using an 8 mm drill bit with approximately 2 mm between the windows. The edges of the window frames were smoothed and 5 smaller 1.5 mm diameter holes bored for use for suturing the frame to the dorsum of the mouse.

2.4 Animals

Female 5 to 7 week old SKH1 mice (24 ± 4g) were obtained from Charles River Laboratories and used in all experiments of this project. One unique characteristic of this murine strain is the loss of hair around three weeks of age, a characteristic similar to alopecia [37]. This phenotypic characteristic was a desirable feature for trans-illumination of the skin for observation of microvessels at weekly intervals. Mice were housed in the Missouri S&T Animal Research Facility with free access to both food and water. Animal protocols used in this project were pre-approved by the Missouri S&T Animal Care and Use Committee and complied with all regulations of Office of Laboratory Animal Welfare (OLAW). NIH guidelines for the care and use of laboratory animals (NIH Publication #85-23 Rev. 1985) have been observed.

2.5 Surgical procedures

In preparation for surgery the animals were anesthetized by intraperitoneal injection of a mixture of ketamine (16.7 mg/kg), xylazine (4 mg/kg), and acepromazine (2 mg/kg). The dorsal surface of the mouse was disinfected with Betadine surgical scrub followed by 70% alcohol. The mouse was placed on a sterile drape covering a controlled-temperature stainless steel tray which was used to prevent a drop in body temperature during anesthesia. Light was transmitted through a lifted fold of dorsal skin via a bifurcated light source (Fostec Model 3115PS) to identify location of large vessels

(as shown in Figure 2A). An indelible mark was made at the center point between the major vessels for use as a reference when subsequently installing the skin window frame. Fine scissors were used to make two 3 mm transverse incisions in the dorsal skin approximately 8 mm cranial and 8 mm caudal to the reference mark. Phosphate buffered saline (PBS; 3 µl) was pipetted into the incision to act as a lubricant to aid insertion of the glass microdispenser delivery tube. After inserting the delivery tube, a sterile stainless steel rod was used to displace the bioactive glass plug from the tube. A second plug was implanted 8 mm caudally. The incision was closed using a minimal amount of superglue.

Following implantation of the glass microfiber plugs, a pre-sterilized dorsal window frame was aligned such that the bioactive glass plugs were approximately in the middle of each window of the frame. The two sides of each dorsal window frame were sutured together with Ethicon 4-0 black nylon monofilament to hold the frame securely in place and prevent movement (as shown in Figure 2B). Ketoprofen was administered subcutaneously at a dose of 5 mg/kg following the completion of the surgery for pain management.

The steps in the surgical implantation of the fused glass beads were performed similarly to those used for the glass microfiber plugs. A single transverse 3 mm incision was made at the mid-dorsal reference mark and PBS pipetted into the incision to act as lubricant. A sterile bead was aseptically positioned at the lip of the incision and a sterile 200 µl pipette tip used to push the bead into the incision and approximately 8 mm cranially. The second bead was similarly positioned and pushed into the incision approximately 8 mm caudally. A dorsal window frame was then placed over the dorsal skin fold, aligned with the implanted beads approximately in the middle of each window,

and sutured into place as described above. The remaining steps of implantation were similar. Following the completion of the surgical implantation and attachment of the dorsal skin window frames, each animal received a subcutaneous injection of Ketoprofen, 5 m/kg, for pain management.

2.6 Live imaging through dorsal skin window

A plexiglass platform (approximately 25 cm x 35 cm) with 15 cm high support leg was used during digital imaging of live tissues enclosed in the skin window frames. To begin the imaging, an alert animal was placed in a tubular restraint device which was then placed on the plexiglass viewing platform with the animal positioned on its side. A light pipe below the platform was adjusted to project light through the skin enclosed in the window frame. The focus ring of the 10x macrozoom affixed to the digital camera mounted above the platform was adjusted to bring the trans-illuminated skin fold into focus and digital images of the tissue were collected.

2.7 Tissue collection and processing for histology

At the conclusion of the three week implantations, animals were euthanized by CO_2 inhalation and the entire segment of whole skin at each implantation site was excised with an 8 mm biopsy punch (Miltex). Immediately following excision, the implant material (bead or plug) was carefully removed from the excised disc and the skin sample then placed in ten volumes of 10% neutral buffered formalin. Following a four day soak, the fixed tissue samples were rinsed in PBS and dehydrated through a graded series of ethyl alcohol solutions. The fully dehydrated tissues were place in a programmable vacuum tissue processor (Tissue-Tek Model VIP2000) for infiltration with paraffin. The paraffin embedded samples were then sectioned at a thickness 5 µm with a Leica model

RM 2235 microtome and the resulting tissues sections mounted on positively charged microscope slides.

2.8 Histological evaluation and microscopy

Microscope slides containing the paraffin thin sections were deparaffinized in xylene for five minutes followed by hydration in distilled water in preparation for periodic acid Schiff (PAS) staining, the method chosen for histological definition of the subcutaneous tissue samples. The hydrated tissue sections were immersed for five minutes in 0.5% periodic acid solution, washed in distilled water, and then submerged in Schiff reagent for 17 minutes followed by two washes (30 seconds each) in 0.55% potassium metabisulfite to remove excess Schiff stain. Sections were then placed in room temperature tap water to develop full color followed by 30 seconds of counter staining with 1% solution of light green. Stained sections were washed with distilled water, dehydrated in ethyl alcohol, cleared for five minutes in xylene, and a cover slip mounted with synthetic resin (Permount-Fischer). This sequence caused the endothelial basal lamina to stain dark blue by the PAS solution while erythrocytes were stained green by the 1% light green counterstain thereby facilitating visualization of the microvasculature [38].

The stained slides tissue sections were then examined by bright field illumination under an Olympus BX53 microscope fitted with an Olympus DP70 camera. The entire tissue sample section (approximately 8 mm x 8 mm) was initially imaged with a 4x objective which was used to obtain overlapping 4x digital images. The ‘Photomerge’ tool of Adobe Photoshop CS3 was used to merge these images into one large composite image of the entire stained section of tissue. Using other features of the Photoshop CS3

software, the composite images was overlaid with a grid pattern. As explained in the appendix, the grid was designed such that the area of the individual boxes of the grid corresponded to the field of view seen under the 20x objective of the microscope. Using the randomized selection scheme described in the Appendix, four separate boxes for each tissue section were randomly selected for collection of the higher resolution digital images with the 20x objective.

2.9 Image analysis and histomorphometry

ImageJ software was used for histomorphometric analysis of the four 20x digital images of each tissue sample. The histomorphometry was started by making two electronic copies of each digital image. The 'pencil tool' in the ImageJ program was used to encircle all PAS-stained vessels visible in copy one, as shown in Figure 3. In a similar manner all void areas without tissue were encircled in copy two. The pictures were converted to binary images and further processed by using the 'Analyze' function to measure the percentage of vessel area in copy one and the void area in copy two. Void areas were subtracted from the total area (if applicable) and a percentage of vessel area to total tissue area was calculated. The following equation was used to quantitatively compare each of the different treatment glasses.

$$\% \text{ Vessel area} = (\text{Vessel Area} / \text{Total Area-Void Area}) \times 100$$

2.10 Extraction of total RNA

A modified procedure of Chomczynski & Sacchi [39,40] was used to isolate total RNA with strict attention to precautionary steps to avoid degradation of RNA by inadequate cooling, contamination with RNases, and other problems. Immediately following euthanasia by CO_2 inhalation, full thickness skin at the implant site was quickly

excised with an 8 mm biopsy punch and snap frozen in liquid nitrogen. The 10 mg treatment beads were removed from the frozen tissue samples prior to pulverization. Working under liquid nitrogen in a pre-chilled mortar and pestle, each frozen tissue was pulverized into a fine powder that was placed in a 1.5 ml RNase-free microfuge tube and held at -80^{o}C. The pulverized tissue in each microfuge tube received a 400 µl volume of guanidinium thiocyanate-phenol-chloroform extraction solution (TRIzol®) in which the tissue was thoroughly homogenized using a motorized dental hand drill (Aseptico model AEU-10) fitted with a disposable RNase-free pestle. Chloroform was added to the TRIzol homogenate mixture which was separated to two phases by centrifugation at 12,000 x g. The upper aqueous phase was withdrawn and isopropyl alcohol added to precipitate RNA which was then pelleted by centrifugation at 10,000 x g. The gel-like pellet containing RNA was washed twice in RNase-free ethanol, partially dehydrated, and finally suspended in 40 µl diethylpyrocarbonate (DEPC) treated water. Aliquots of each sample were analyzed with a Nanodrop 3000 spectrophotometer to measure absorbance at 260 nm and 280 nm for determination of A_{260}/A_{280} ratio. Samples of total RNA (1 µg) were also run on a 1% agarose/formaldehyde denaturing gel and, after the electrophoresis run, were stained with SYBR-Gold nucleic acid stain. The agarose gel containing total RNA aliquots was imaged to assess sharpness of the 18S and 28S bands of ribosomal RNA and the extent of smearing.

2.11 Analysis of gene expression by quantitative PCR

Advance arrangements were made with an outside contract laboratory associated with the Mouse Biology Program at the University of California-Davis for analysis of gene expression by quantitative PCR (qPCR). Total RNA samples were packaged in dry

ice and shipped overnight to the UC-Davis lab. The 12 RNA samples sent for analysis included three samples of RNA from sham control tissues along with three samples of RNA from week one, week two, and week three tissues treated with the 13-93B3Cu glass. The samples were initially converted to cDNA. Custom constructed oligonucleotide probes (TaqMan® probes) specific for the VEGF and FGF-2 target genes plus the GAPDH gene (which was used as an endogenous control) were synthesized by the UC-Davis lab in preparation for their qPCR assays of gene expression. The special attribute of these TaqMan® probes is the inclusion of both a fluorophore and a quencher moiety in the same molecule. Taq polymerase reaction mix plus duplicate aliquots from each sample along with duplicate aliquots of each of each TaqMan® probe were pipetted in the wells of a multiwall plate which was then placed in the qPCR thermal cycler instrument. As product cDNA is amplified by the thermal cycling, the TaqMan® probe is degraded to release the fluorophore which is then fluorescently excited by the instrument light source. The thermal cycle at which the concentration of amplified product cDNA is sufficient for detection above background is designated Ct (threshold cycle), one of the units of measurement in the qPCR procedure [41]. The levels of gene expression of target genes of each sample were compared to that of the GAPDH endogenous control gene. The inclusion of an endogenous control, which is assumed to be uniformly expressed in all tissue samples, was used to obtain ΔCt values [42]. Delta Ct values were calculated by subtracting the control sample Ct value from the endogenous GAPDH control Ct value. Using ΔCt values relative changes in gene expression were also compared by using the delta-delta Ct calculation (as explained in the Appendix) [42].

2.12 Statistical analysis

Data sets are presented as means ± standard error of the mean (SEM). Evaluation of treatment groups from experiments was done by one way analysis of variance (ANOVA) followed by the Tukey post-hoc test to identify significant differences between treatment groups. Differences between group means were considered significant with p-values less than 0.05 ($p< 0.05$) and moderately significant with p-values less than 0.10 ($p< 0.10$).

III. RESULTS

3.1 Imaging of localized tissue response to bioactive glass implants

The materials initially used for implantation in dorsal skin window preparations for live imaging of localized tissue responses were compressed plugs of microfibrous glass. It soon became clear, however, that the microfibrous plugs were injurious to the local tissue. Signs of tissue injury that were seen in response to the microfibrous plugs included the accumulation of pockets of fluid edema accompanied by an inflamed reddish appearance in the surrounding tissue. The development of an inflamed appearance was an unwanted artifact that would complicate the visualization of tissue responses including the possible formation of new microvessels resulting from angiogenesis. In an effort to reduce or eliminate the inflammatory response artifacts, it was decided to use spherical beads of fused glass in subsequent implantations for live imaging. The rationale for switching to fused beads was the premise that the smooth surface of the beads would likely be less irritating than plugs of compressed glass microfibers, many of which have exposed sharp ends that would cause tissue irritation.

Representative live macroscopic images of localized tissue responses to bioactive glass beads implanted in dorsal skin window preparations and subsequently photographed at one, two and three weeks after implantation are shown in Figures 4, 5, and 6, respectively. Not included here are day zero images that were obtained within 30 minutes after implantation of the fused beads. The day zero skin window photos showed minor inflammation that formed quickly around some of the fused beads although this minor inflammation appeared to subside before the follow-up week one photos were taken. Figure 4 shows an image representative of the dorsal skin windows at week 1

post-implantation. There was little or no observable response with any of the implanted beads except for minor redness surrounding one of the implanted 13-93B3Cu beads and one 13-93B3 bead. The representative images in Figure 5 of tissue response at week 2 show a halo-like body surrounding a 13-93B3 bead and an even more prominent halo around a 13-93B3Cu bead. The halos around the beads at week 2 extended approximately 1 mm beyond the edge of the bead, a finding also observed with the other borate beads that were implanted. The representative week 3 skin window sample shown in Figure 6 reveals a clear difference in response to the borate-based glass bead and the silicate-based glass bead. The borate-based 13-93B3 bead has a distinct and localized halo response around the implant. In contrast, the silicate-based 13-93 glass beads produced little or no discernable response. Overall, the outcome of the live imaging was the finding of essentially no new vessels nor increased microvascular density visible in tissue surrounding the 13-93 glass beads while tissues implanted with the borate-based 13-93B3 and 13-93B3Cu beads showed increased redness and halo formation. A tabulated summary of qualitative scoring of the responses of soft tissue to borate and silicate-based beads in dorsal skin windows is presented in Table II. As indicated in the table, a distinct halo-like body was observed around only one of the five 13-93 silicate glass beads at week 3. In contrast, distinct halos were observed at week 3 around three of the five implanted 13-93B3 beads and two of the three remaining 13-93B3Cu beads. The halos surrounding the borate-based 13-93B3 and 13-93B3Cu beads had an outer diameter of approximately 3-4 mm, became prominent at week two, and remained distinct until the animals were sacrificed at week three.

In addition to the sample images of response to separate beads as shown in Figures 4-6, the photo images in Figure 7 show a three week progression of tissue responses to an implanted13-93 bead and a 13-93B3 bead. Figure 7A and 7B show week zero pictures obtained within 30 minutes after implantation. Minor inflammation caused by the bead insertion was observed with the 13-93B3 bead, although this subsided before the subsequent photos at week 1. The week 1 response visible in Figure 7C and 7D reveals little or no tissue response around either of the two beads. Figure 7E and 7F compares the localized tissue response around the two different beads at week 2. As shown in this comparison, there is a prominent halo response around the borate-based 13-93B3 bead but not around the 13-93 bead. The tissue responses appear virtually the same at week 3 as shown in Figures 7G and 7H. Another interesting morphological feature noticed in this three week sequence of photos is an increasing prominence of the large vessels near the 13-93B3 bead.

A follow-up side experiment was conducted to further characterize the halo structures. The follow-up included a separate group of 10 SKH1 mice that received subdermal implantations of 13-93, 13-93B3, and 13-93B3Cu fused beads without the use of the skin window frames. The objective of this approach was macroscopic viewing of tissue responses in a more direct manner from the subdermal side of necropsied skin rather than by repeat indirect viewing from the epidermal side of intact live skin enclosed within the dorsal skin window preparations. Three weeks after implantation, the animals were euthanized, a mid-dorsal incision was made, and the skin reflected for direct, macroscopic photo imaging of subdermal soft tissue. Three of the four sham implantation sites were no longer detectable when examining the subdermal surface at

three weeks post implantation while at the one sham site that was still somewhat discernable there was only a very small (<1 mm diameter), slightly reddish body. The outcome with the beads, as shown by the photo images in Figure 8, was the finding of a reddish, halo-like structure surrounding each of the four implanted 13-93B3Cu beads and each of the four implanted 13-93B3 beads but no similar halo response at any of the four sites with 13-93 beads. As shown, the halo-like structures surrounding the 13-93B3Cu beads were more intense than the halos surrounding the 13-93B3 beads. It was noticed that the distinct halo around the 13-93B3Cu beads included well delineated microvessels. Furthermore, the halo structures around 13-93B3Cu beads (as viewed here from the subdermal surface of the necropsied skin) were about 4 mm in diameter and similar to the halo-like structures observed from the epidermal side in the live dorsal skin window preparations. In addition to the tissue response, the physical appearance of the implant was also observed. At three weeks post implantation the glass beads were intact, appeared to be the same diameter as when initially implanted, and had no noticeable reacted layer on their surface.

3.2 Sample recovery and histological evaluation of soft tissue response

At conclusion of the three week implantation, discs of whole skin were excised from the dorsal skin fold preparations and the implants immediately examined. The microfiber plug appeared approximately the same size after three weeks but was covered with a thin white reacted layer. In addition, the plugs were soft, moist, and crumbled upon removal. The glass beads appeared to be the same diameter as when initially implanted, they were completely intact upon removal, and there was no observable white reactive layer on their surface. After processing and staining the tissue samples, digital

photos were taken with the 4x objective of separate area of the stained tissue sections and the 4x images digitally combined to form a low magnification, composite image of the entire tissue section as explained in the Materials and Methods. An example of this is the image shown in Figure 9, a composite image of tissue from a dorsal skin fold preparation implanted with a 13-93B3Cu bead. Included in the figure are two enlarged areas that show the relative density of microvessels at the periphery (Figure 9A) of the tissue section and also near of the former site of the implanted bead (Figure 9B). Comparison of the two enlarged areas appears to show a higher density of microvessels proximal to the bead. This finding is consistent with the microvessel-containing halo that was observed around each of the 13-93B3Cu beads that were seen both in the live skin window preparations and in the necropsied skin samples as described above.

Using the randomized selection procedure mentioned in Materials and Methods (and described in detail in the Appendix), four fields within each tissue section were selected for digital imaging at higher magnification through the 20x objective. The four panels of Figure 10 show representative 20x images of PAS-stained sections of subdermal tissues removed three weeks after implantation of fused glass beads. The sham control sample shown in Figure 10A, which is representative of the subdermal tissues recovered from sites where no bead was implanted, shows adipose and areolar tissues with a low microvascular density. The image in Figure 10B is a representative example of tissue with the silicate-based 13-93 glass bead. The tissue shown here has a microvascular density that is similar to that of sham control tissue. Microvessels can be seen along with fibrous tissue on the right side of the image. Sections of soft tissues from the 13-93B3 and 13-93B3Cu implantation sites are shown in Figures 10C and 10D,

respectively. The tissue with the borate-based 13-93B3 bead (Figure 10C) appears to contain increased fibrous tissue plus a qualitatively higher density of microvasculature. The tissues from implants sites with the 13-93B3Cu glass appeared qualitatively to contain the highest density of microvessels. Minor amounts of fibrous tissue were observed throughout tissues with the 13-93B3 and 13-93B3Cu beads, a finding representative of other replicates. Many of the small microvessels visible in Figure 10D appear approximately the same diameter as an erythrocyte indicating that they are capillaries. The histological evaluation revealed that the replicate tissue samples recovered from the other sites of implantation of 13-93B3Cu glass beads also appeared qualitatively to have the highest density of microvessels.

The four panels of Figure 11 show representative 20x images of PAS-stained sections of subdermal tissues removed three weeks after implantation of glass microfiber plugs. Figure 11A is representative of the subdermal tissues recovered from sham control sample. This panel shows adipose and areolar tissues with a low microvascular density and is similar to the sham control samples above. The image in Figure 11B is a representative example of tissue implanted with silicate-based 45S5 glass microfibers. The section shown here has a tissue composition similar to that of sham control sample and a similar microvessel density. Representative images of soft tissues from the sites of implantation of 13-93B3 and 13-93B3Cu glass microfibers are shown in Figures 11C and 11D, respectively. The image in Figure 11 of tissue with the borate-based 13-93B3 glass microfibers appears to qualitatively show a slightly higher microvessel density, a difference also discernable in the other tissues with this type of glass microfibers. The tissues from implants sites with the 13-93B3Cu glass qualitatively appeared to contain

the highest density of microvessels as localized tissue response. Moderate amounts of fibrous tissue were observed in tissues with both types of borate-based microfibrous plugs. More microvessels can be observed in all of the treatment tissues with microfibrous plugs, but the 13-93B3Cu glass microfibers appeared qualitatively to promote the highest microvessel density in the surrounding tissue. As in the case above, the histological evaluation revealed that the replicate tissue samples recovered from the other sites with 13-93B3Cu glass microfibers also appeared qualitatively to contain the highest density of microvessels.

3.3 Quantitative histomorphometry

A summarized comparison of the microvessel density in soft tissue recovered from the sites of implantation of bioactive glass beads and glass microfiber plugs is presented in Table III. The quantitative histomorphometric measurements reveal that all implantations of bioactive glass, both in the form of beads and in the form of compressed microfiber plugs, resulted in higher microvessel densities than those of the sham control tissues. The total vessel areas observed in the two groups of sham control tissues were both calculated to be 2.6% of the total observed tissue area. Implantation of the fused glass beads and glass microfiber plugs resulted in the same overall trend for the tissue microvessel densities which were observed to be: lowest in the sham control tissues; slightly higher in tissues with silicate-based 13-93 or 45S5 glass; higher yet in tissues with 13-93B3 glass beads and glass microfibers; followed by the highest microvessel densities in tissues with 13-93B3Cu glass beads and glass microfibers. The tissues implanted with the 13-93, 13-93B3, and 13-93B3Cu glass beads showed 33%, 58%, and 145% higher microvessel density values relative to the three-week sham control tissues,

respectively. In a similar manner, the tissues containing 45S5, 13-93B3, and 13-93B3Cu glass microfiber plugs were found to have microvessel densities that were 56%, 124%, and 171% higher, respectively, compared to the three week sham control tissues.

The two bar charts in Figure 12 provide graphical representation of the mean microvessel densities with statistical analysis of differences between the treatment groups. Results of the ANOVA test revealed the differences between the mean values of the various groups were greater than would be expected by chance and significant at the $p<0.05$ level. A Tukey HSD post-hoc test was performed as a follow up to test for significant differences between individual treatment groups. The Tukey test indicated that the higher microvessel densities of soft tissues with 13-93B3Cu glass beads or glass microfiber compared to microvessel densities of the sham control tissues was statistically significant at the $p<0.05$ level. The higher microvessel densities of tissues with 13-93B3 glass beads or glass microfiber compared to sham control tissues were found to be marginally significant at $p<0.10$. In contrast, the microvessel densities of tissues with silicate-based 45S5 and 13-93 glasses were not statistically different than those of the sham control tissues.

3.4 Analyses of total RNA extracts

The yields of total RNA extracted from the frozen skin samples were, as expected, rather low with values ranging from 120 ng/µl to 276 ng/µl for aliquots suspended in DEPC-treated water. The integrity of the total RNA extracts was evaluated by spectrophotometry and gel electrophoresis. The average A260/280 ratios for total RNA from sham control and from the 13-93B3Cu wk1, 13-93B3Cu wk2, and 13-93B3Cu wk3 skin samples were 1.88, 1.85, 1.82, and 1.87, respectively. Aliquots (1 µg each) of

total RNA were loaded on 1% agarose/formaldehyde denaturing gels, subjected to electrophoresis, and the resultant separated bands then stained with the nucleic acid dye SYBR-Gold. Figure 13 shows a representative 1.0% agarose formaldehyde gel loaded with 1µg of total RNA in one lane plus an aliquot of standard 500-9,000 base oligonucleotide ladder in a separate lane. As shown, there are two intense bands at approximately 5 kb and 1.9 kb that correspond to 28S rRNA and 18S rRNA, respectively, plus a near absence of smearing. The presence of sharp 18S and 28S bands along with nearly complete absence of smearing was also seen in all of the other preparations of total RNA extracted from frozen skin samples, findings that confirm the integrity of the RNA preparations.

3.5 qPCR analysis of gene expression

The results for all qPCR gene expression assays were obtained by an outside contract laboratory associated with the Mouse Biology Program at the University of California-Davis. The assays were performed on twelve RNA samples that included three samples of sham control RNA along with three samples of RNA from week one, week two, and week three tissues treated with the 13-93B3Cu glass beads. As indicated in the Materials and Methods section the RNA samples were converted to cDNA through reverse transcription and custom TaqMan® probes specific for VEGF and FGF-2 target genes plus the GAPDH endogenous control gene were synthesized by the UC-Davis lab. Duplicate aliquots of the probes, cDNA from each sample, and other necessary reaction components were pipetted into the wells of a multiwall plate and placed in a thermal cycler instrument. As the qPCR continues and newly-formed product cDNA matching the target gene is synthesized, florescence is detected at a critical threshold (Ct) as explained

in Section 2.11. The thermal cycle number at which Ct is reached was determined. The Ct values of VEGF, FGF-2, and sham control were normalized to the Ct values of endogenous GAPDH controls. Gene expression values are then listed as delta-Ct values (as given in Table IV), or the Ct difference between the endogenous control and target genes. Relative FGF-2 expression showed changes at weeks one through three of 0.53, 0.81, and 0.93, respectively (shown in Figure 14A) with no statistically significant difference compared to the sham control. VEGF expression showed fold changes of 0.78, 1.12, and 1.80 during weeks one through three, respectively, as shown in Figure 14B. Statistical analysis, including a one way analysis of variation (ANOVA) followed by a student t-test was performed on the delta-Ct values from each treatment group. The VEGF expression data showed that there was marginally significant difference at the $p < 0.10$ level ($p = 0.057$) between the sham control and 13-93B3Cu week 3 values.

IV. DISCUSSION

Current procedures and materials for wound treatment have yielded relatively poor outcomes with chronic skin wounds, a major health care challenge. In that sense, the new treatment procedure recently tested in a clinical study at the Phelps County Regional Medical Center (PCRMC) is a noteworthy exception. This new procedure involved treatment of venous stasis wounds with dressings composed of borate-based glass microfibers [35]. The results of the PCRMC clinical trial were a dramatic improvement in the healing of previously non-responsive wounds for most of the volunteers enrolled in the study. The borate-based glass microfiber treatments were very encouraging, but mode of action in the wound healing process was not addressed. Related rodent model studies from two different laboratory groups at Missouri S&T investigated the possible angiogenic effects of bioactive borate-based glass materials. One study involving subcutaneous implantation of sintered glass fiber scaffolds reported an increased density of vessels around and within scaffolds composed of copper-doped borate glass fibers compared to those without copper [43]. The second study reported a dramatic increase in the microvessel density of subcutaneous tissues with borate-based glass microfiber implants compared with sham-implanted, blank control tissues [36]. Both projects revealed an angiogenic effect of the borate-based glasses although the underlying mechanism of angiogenic effect was not investigated.

This project was undertaken to specifically address the physiological and molecular mechanism of the angiogenic effect of borate-based glass materials. An original intention in the use of trans-illuminated skin window preparations was to achieve

sufficient resolution for clear delineation of microvessels that might form in response to the implant. The level of resolution that was obtained during live imaging through the skin folds was not sufficient to permit consistent delineation of microvessels. As a consequence, the live images were not suitable for quantitative histomorphometric measurements with image analysis software. The imaging did, however, allow unambiguous recognition of differences in the extent of the soft tissue responses to the borate-based glass beads and the silicate-based glass beads which were assessed qualitatively. As described in the Results section, much of the live soft tissue response observed around the borate-based beads involved the formation of a halo body. In the few images with sufficiently high resolution, the halo bodies were recognized to be tissue clusters infused with microvessels. And, the formation of microvessel clusters or halo bodies observed around the 13-93B3 and 13-93B3Cu beads is consistent with the formation of granulation tissue that was observed in the PCRMC clinical study [35].

The interpretation that the halo observed in the live image were mostly composed of microvessel-rich soft tissue was supported by the necropsy images obtained at 3 weeks post-implantation. The necropsy examination revealed clearly delineated microvessels visable within the reddish mass found around some of the implanted beads. Furthermore, the reddish mass encircling the borate-based glass beads of the necropsy samples was approximately the same size as the halo bodies observed during live imaging of the dorsal skin folds, appeared most prominent around the 13-93B3Cu glass bead, and virtually absent with the silicate-based 13-93 glass beads. Also noticed in the necropsy samples were vessels ‘budding’ toward some of the 13-93B3Cu glass bead, an indication of angiogenesis.

The results of histological evaluation of the PAS-stained tissue sections also support the interpretation that the halo bodies surrounding the borate glass beads were tissue clusters infused with microvessels. As mentioned, the microvessel densities observed here were found to be higher within about a millimeter of the implanted borate bead compared to areas distal to the bead. This finding agrees with the higher microvessel densities observed around subcutaneously implanted plugs of 13-93B3Cu glass microfibers as reported in the related similar *in vivo* investigation by Lin *et al*. [36]

Close inspection of the table of histomorphometry results reveals a difference in the extent of the angiogenic response to glass microfibers plugs and beads. Higher microvessel densities were observed around the microfibrous plug than the fused glass bead. This difference can in part be attributed to the difference in surface area of the two physical forms of the glass implants. The plugs composed of borate glass microfibers with nominal diameters of approximately 2-5 μm have a much higher surface area than the 2 mm in diameter. The micron diameter fibers react completely in three weeks [34,43] releasing all of the boron and copper. The glass bead did not appear to have a reacted surface layer, another indication of slower dissolution.. Due to the diameter of their component fibers together with moderate porosity, the microfibrous plug would have a vastly higher surface area which contributes to fast dissolution resulting in higher localized concentrations of borate and copper, the angiogenic ions [44-47].

The extent of the angiogenic response to the borate glass plugs and beads used in this study was about two-thirds of level of the angiogenic effect of microfibrous bioactive borate glass used in the previous study by Lin [36]. This reported difference in angiogenic response may in part reflect the different methods of randomly selecting

candidate areas for measurement of vessel densities in the stained slides. The method used in this project involved randomly selecting candidate fields from a grid overlay composite image of the entire sample. In contrast, the method used in the previous study involved unbiased selection of areas that were within approximately a millimeter of the microfibrous glass implant [36]. The inclusion of area for enumeration distal to the implant, as was done in this project, would quite clearly cause the overall observed angiogenic effect to be less.

The effects of borate-based bioactive glass on expression of vascular endothelial growth factor (VEGF) *in vivo* had not been investigated prior to this study. Thus, an important and novel aspect of this investigation is the finding of elevated expression of VEGF mRNA in skin tissue after three weeks with the 13-93B3Cu glass beads in place. Many growth factors have been shown to be involved in wound healing, but VEGF has been identified as having an especially important role [48]. And, the 13-93B3Cu beads did trigger a 1.8-fold increase in VEGF expression after three weeks. Fibroblast growth factor-2 (FGF-2) has also been reported to be important in vasculogenesis [55]. However, the results of this study indicated there was no increase in expression of FGF-2 mRNA in response to the 13-93B3Cu glass beads. The relatively modest increase in VEGF expression after three weeks in response to the 13-93B3Cu beads is likely related to a slower dissolution of the glass beads. It might be anticipated that a higher level of VEGF expression would likely occur in response to implantation of more rapidly dissolving 13-93B3Cu glass microfiber plugs.

Collectively, the results of this project demonstrate that the borate-based bioactive glass beads and microfiber plugs do promote angiogenesis, an essential step in wound

healing. These positive results provide additional evidence that these materials are potentially useful for treating chronic non-healing wounds. An important outcome was the finding that copper-doped 13-93B3Cu glass is able to stimulate VEGF expression which would promote angiogenesis. This finding suggests a bioactive borate glass implant would be a simple but effective vehicle for delivery of pro-angiogenic ions and, as a result, an attractive alternative to expensive growth factors for treatment for chronic wounds. Additional work is needed to determine if expression of other angiogenic cytokines might also occur as part of the response of soft tissue to 13-93B3 bioactive glass doped with various leachable ions.

V. CONCLUSION

The live imaging of dorsal skin window preparations in the hairless SKH1 showed the formation of a halo-like structure infused with vessels in soft tissue surrounding borate-based 13-93B3 and 13-93B3Cu glass beads two weeks after implantation. This response was not observed around silicate-based 13-93 glass beads. Histological examination of the soft tissue recovered three weeks after implantation revealed statistically significant increase (state them) in the microvessel density at implant sites with 13-93B3Cu glass microfibers. Quantitative PCR measurements indicate a marginally significant increase in expression of VEGF mRNA in skin tissues with 13-93B3Cu. This latter outcome partially marginally supports the project hypothesis that 13-93B3Cu glass induces VEGF expression followed by neovascularization, a key process of wound healing.

PROJECT FUNDING AND SUPPORT

This investigation was supported by funds from the Center for Biomedical Sciences and Engineering at Missouri University of Science and Technology. The bioactive glass materials used in this study were donated by the MO-Sci Corp in Rolla, MO.

APPENDIX A

Procedure for random selection of grid overlay areas for measuring microvessel density

Each stained tissue section was initially imaged under the 4x objective and multiple overlapping 4x digital images were obtained to form one large composite image of the entire tissue section. A sequentially numbered grid pattern created with Microsoft PowerPoint was then over layered onto the composite 4x image as shown in Figure 15B. The grid was scaled such that individual boxes of the grid cover an area equivalent to the field of view under the 20x objective. Each field within the grid was examined under the 20x objective to assess relative amounts of subdermis, the skin layer in which the microvasculature is located. Fields containing less than 50% subdermis were excluded. Also excluded from the grid were boxes devoid of tissue. For the example presented here, the remaining candidate fields are those corresponding to the remaining numbered boxes shown in Figure 15C. The numbers identifying the candidate fields were entered in a Microsoft Excel file and the '=RANDBETWEEN' function of Excel then used to randomly select four numbers from the file. For the example presented here, the four fields selected (i.e., the four 20x fields randomly selected for quantitative measurement of microvessel density) are indicated by the highlighted numbers boxes shown in Figure 15D.

APPENDIX B

The delta-delta Ct calculation

The delta-delta Ct (comparative CT calculation method) is a method of quantitation of relative gene expression [42]. Total RNA is converted into complementary DNA (cDNA) through polymerase chain reaction (PCR) which amplifies specific target regions of cDNA through repeated cycles of separation and annealing the two strands of DNA. The first step in the determination of relative gene expression is quantitating the fractional number of thermal cycles at which a detectable signal is observed for the target genes (VEGF and FGF-2) in the PCR process. This number of cycles at which the target region of cDNA is sufficiently amplified is designated the Ct value (threshold cycle). The Ct value is somewhat are counterintuitive because the lower the Ct value the greater the amount of starting material (mRNA template for the target gene) in the sample. The average Ct value is calculated for both the target genes and the endogenous GAPDH control gene. The difference between the endogenous control and the target gene is designated ΔCt and is equal to the mean Ct value for each target gene minus the mean Ct value for the endogenous GAPDH control. This ΔCt value is the basis for all subsequent data transformations via the delta-delta Ct calculation. Each ΔΔCt value represents the difference between the ΔCt value for a target gene in a treated tissue sample minus the ΔCt value for the same target gene in a sham control tissue sample. Finally, a 2^(-ΔΔCt) value is calculated by the equation below:

2^(-ΔΔCt) where ΔΔCt = ΔCt treated tissue – ΔCt control tissue

In typical cases in which the ΔCt value of the treated tissue is less than the ΔCt value of the control tissue, the ΔΔCt value is negative and the resultant 2^(-ΔΔCt) value is positive. The calculation of 2^(-ΔΔCt) values is now widely used by the numerous research laboratories that routinely measure gene expression levels. Additionally, it has

been established that calculated 2^(-ΔΔCt) values are approximately equivalent to the fold-change difference in gene expression as calculated by quantitative comparison to a standard curve with known amounts of cDNA standard [41].

REFERENCES

[1] Chandan SK, Gordillo, MG, Sashwati R, Kirsner R, Lambert L, Hunt TK, Gottrup F, Gurtner GC, Longaker MT. Human skin wounds: a major and snowballing threat to public health and the economy. Wound Repair Regen. 2009; 17: 763–771.

[2] Wu SC, Driver VR, Wrobel JS, Armstrong, DG. Foot ulcers in the diabetic patient, prevention and treatment. Vasc Health Risk Manag. 2007; 3: 65–76.

[3] Caputo G, Cavanagh P, Ulbrecht J, Gibbons G, Karchmer A. Assessment and management of foot disease in patients with diabetes. N Engl J Med. 1994; 13: 854-860.

[4] Falanga V. Wound healing and its impairment in the diabetic foot. Lancet 2005; 366: 1736-43.

[5] Tonnesen M, Feng X, Clark R. Angiogenesis in wound healing. J Invest Dermatol Symp Proc 2000; 5: 40–46.

[6] Waugh H, Sherratt J. Macrophage dynamics in diabetic wound healing. Bulletin of Mathematical Biology 2006; 68: 197-207.

[7] Gurtner GC, Werner S, Barrandon Y, Longaker, MT. Wound repair and regeneration. Nature 2008; 453: 314-321.

[8] Olson JK, Miller SD. Microglia initiate central nervous system innate and adaptive immune responses through multiple TLRs. J Immunol 2004; 173: 3916-3924.

[9] Stroncek JD, Reichert WM. Overview of wound healing in different tissue types. In: Reichert WM, editor. Indwelling neural implants: strategies for contending with the *in vivo* environment. Boca Raton (FL): CRC Press; 2008. Chapter 1.

[10] Keshaw H, Forbes A, Day RM. Release of angiogenic growth factor from cells encapsulated in alginate beads with bioactive glass. Biomaterials 2005; 26: 4171-4179.

[11] Barralet J, Gbureck U, Habibovic P, Vorndran E, Gerard C, Doillon CJ. Angiogenesis in calcium phosphate scaffolds by inorganic copper ion release. Tissue Eng 2009; 15: 1601-1608.

[12] Li J, Zhang YP, Kirsner, RS. Angiogenesis in wound repair: Angiogenic growth factors and the extracellular matrix. Micros Res Tech 2003; 60: 107-114.

[13] Cole RW, Liu F, Herron BJ. Imaging of angiogenesis: past, present and future. Microscopy: Science Technology, Applications and Education 2010; 1 :885-896.

[14] Folkman J, Shing Y. Angiogenesis. J Biol Chem 1992; 267: 10931-10934.

[15] Shih SC, Robinson GS, Perruzzi CA, Calvo A, Desai K, Green JE, Ali IU, Lois E, Smith H, and Senger, DR. Molecular profiling of angiogenesis markers. Am J Pathol 2002; 161: 35-40.

[16] Clayton W, Elasy T. A review of the pathophysiology, classification, and treatment of foot ulcers in diabetic patients. Clin Diabetes 2009; 27: 52-58.

[17] Mohammad G, Pandey H, Tripathi K. Diabetic wound healing and its angiogenesis with special reference to nanoparticles. Dig J Nanomat Biostruc 2008; 3: 203–208.

[18] Demidova-Rice TN, Durham JT, and Herman IA. Wound healing angiogenesis: innovations and challenges in acute and chronic wound healing. Adv Wound Care. 2012; 1: 17–22.

[19] Papanas, N, Efstratios M. Becaplermin gel in the treatment of diabetic neuropathic foot ulcers. Clin Interv Aging. Jun 2008; 3(2): 233–240.

[20] Giavazzi R, Sennino B, Coltrini D, Garofalo A, Dossi R, Ronca R, Pia M, Tosatti M, Presta M. Distinct role of fibroblast growth factor-2 and vascular endothelial growth factor on tumor growth and angiogenesis. Am J Pathol. Jun 2003;162: 1913–1926.

[21] Witkowski JA, Parish LC. Rational approach to wound care. Int J Dermatol 1992; 31:27-28.

[22] Fang RC, Galiano RD. A review of becaplermin gel in the treatment of diabetic neuropathic foot ulcers. Biologics. 2008; 2: 1–12.

[23] Sherman R, Wyle F, Vulpe M. Maggot therapy for treating pressure ulcers in spinal cord injury patients. J Spinal Cord Med 1995; 18:71-74.

[24] Caputo G, Cavanagh P, Ulbrecht J, Gibbons G, Karchmer A. Assessment and management of foot disease in patients with diabetes. N Engl J Med 1994; 13: 854-860.

[25] Hutchinson JJ, McGuckin M. Occlusive dressings: a microbiologic and clinical review. Am J Infect Control 1990; 18:257-68.

[26] Witkowski JA, Parish LC. Rational approach to wound care. Int J Dermatol 1992: 31:27-8.

[27] Negative pressure wound therapy devices: technology assessment report. November 2009. Agency for Healthcare Research and Quality, Rockville, MD.

[28] Lipsky BA, Berendt AR. Hyperbaric oxygen therapy for diabetic foot wounds. Diabetes Care. 2010; 33: 1143-1145.

[29] Pandya S, Supe A. Hyperbaric oxygen therapy in diabetic foot. J Postgrad Med 1992; 38:112-114

[30] Boyce ST, Warden GD. Principles and practices for treatment of cutaneous wounds with cultured skin substitutes. Am J Surg 2002; 183: 445-56.

[31] Lorenti A. Wound healing: from epidermis culture to tissue engineering. CellBio 2012; 1; 17-29.

[32] Hoppe A, Mouriñob V, Boccaccini AR. Therapeutic inorganic ions in bioactive glasses to enhance bone formation and beyond. Biomaterials Sci 2013; 1: 254-256

[33] Chen Q**,** Zhu C. Thouas GA. Progress and challenges in biomaterials used for bone tissue engineering: bioactive glasses and elastomeric composites. Progress in Biomaterials. 2012, 1:2

[34] Jung, SB, Ph.D Dissertation, Chapter 2, Rolla, MO: Missouri University of Science and Technology; 2010

[35] Peggy Taylor. Private communication 2012.

[36] Lin, Y, Brown, RF, Jung SB, Day DE. 2014 Angiogenic effects of borate glass microfibers in a rodent model. J Mater Sci Mater Res Part A 2014: 00A:000-000

[37] Benavides F, Oberyszyn TM, VanBuskirk AM, Reeve VE, and Kusewitt DF. The hairless mouse in skin research. J Dermatol Sci. 2009; 53:10-18.

[38] Eliza M, Ben I, Reuven B. Histopathological periodic acid–schiff stains of nail clippings as a second-line diagnostic tool in onychomycosis. Am Journal Dermatopathol 2012; 34: 270-273.

[39] Chomczynski P & Sacchi N. Single-step method of RNA isolation by acid guanidinium thiocyanate-phenol-chloroform extraction. Anal Biochem. 1987; 162:156-9.

[40] Chomczynski P, Sacchi N. The single-step method of RNA isolation by acid guanidinium thiocyanate-phenol-chloroform extraction: twenty-something years on. Nat Protoc. 2006; 1: 581-585.

[41] Wong, ML., Medrano, J.F. Real-time PCR for mRNA quantitation. BioTechniques 2005; 39:75-85

[42] Livak KJ, Schmittgen, TD. Analysis of relative gene expression data using real-time quantitative PCR and the 2-[Delta][Delta]Ct method. Methods, 2001; 25:402-408

[43] Jung, SB, Ph.D Dissertation, Chapter 3, Rolla, MO: Missouri University of Science and Technology; 2010

[44] Kucan JO, Robson MC, Heggers JP, Ko F. Comparison of silver sulfadiazine, povidone-iodine and physiologic saline in the treatment of chronic pressure ulcers. J Am Geriatr Soc 1981; 29: 232-235.

[45] Harris E. A requirement for copper in angiogenesis. Nutr Rev. 2004; 62: 60-64.

[46] Hu G. Copper stimulates proliferation of human endothelial cells under culture. Journal of Cellular Biochemistry 1998; 69: 326-335.

[47] Barralet J, Gbureck U, Habibovic P, Vorndran E, Gerard C, Charles J. Angiogenesis in calcium phosphate scaffolds by inorganic copper ion release. Tissue Engineering 2009; 15: 1601-1609.

[48] Sen, CK. Copper-induced vascular endothelial growth factor expression and wound healing. American Journal of Physiology 2002; 282: H1821-H1827.

[49] Bernatchez PN, Soker S, Sirois GM. Vascular endothelial growth factor effect on endothelial cell proliferation, migration, and platelet-activating factor synthesis is Flk-1-dependent. Journal of Biological Chemistry 1999; 274: 31047-31054.

[50] Araki S, Shimada Y, Kaji K, Hayashi H. Apoptosis of vascular endothelial cells by fibroblast growth factor deprivation. Biochem Biophys Res Commun. 1990; 168:1194-1200.

[51] Klein S, Roghani M, Rifkin DB. Fibroblast growth factors as angiogenesis factors: new insights into their mechanism of action. EXS. 1997; 79:159-192.

[52] Presta M, Moscatelli D, Joseph-Silverstein J, Rifkin DB. Purification from a human hepatoma cell line of a basic fibroblast growth factor-like molecule that stimulates capillary endothelial cell plasminogen activator production, DNA synthesis, and migration. Mol Cell Biol. 1986; 6: 4060-4066.

[53] Moscatelli D, Presta M, Rifkin DB. Purification of a factor from human placenta that stimulates capillary endothelial cell protease production, DNA synthesis, and migration. Proc Natl Acad Sci USA. 1986; 83: 2091-2095.

[54] Wilgus TA, Ferreira AM, Oberyszyn TM, Bergdall VK, Dipietro LA. Regulation of scar formation by vascular endothelial growth factor. Lab Invest. 2008; 88: 579–590.

[55] Emanueli C, Madeddu P. Angiogenesis gene therapy to rescue ischaemic tissues: achievements and future directions. Br J Pharmacol. 2001; 133: 951-958.

Table I- Composition of bioactive glasses used for sub-dermal implantations (composition values listed as wt %)

Glass	SiO_2	B_2O_3	Na_2O	CaO	MgO	K_2O	P_2O_5	CuO
45S5	45.00	0	24.50	24.50	0	0	6.00	0
13-93	53.00	0	6.00	20.00	5.00	12.00	4.00	0
13-93B3	0	53.00	6.00	20.00	5.00	12.00	4.00	0
13-93B3Cu	0	52.79	5.98	19.92	4.98	11.95	3.98	0.40

Table II. Qualitative evaluation of soft tissue response to beads implanted in dorsal skin window preparations.

Implant interval	Bead type	Beads (shams) implanted	Beads (shams) remaining	Fraction with halo	Halo density*
1 wk	none (Sham)	(5)	(4)	0/4	0
	13-93	5	5	0/5	0
	13-93B3	5	5	0/5	0
	13-93B3Cu	5	4	1/4	+
2 wk	none (Sham)	(5)	(4)	0/4	0
	13-93	5	5	0/5	0
	13-93B3	5	5	3/5	++
	13-93B3Cu	5	4	3/4	++
3 wk	none (Sham)	(5)	(3)	0/3	0
	13-93	5	5	1/5	+
	13-93B3	5	5	3/5	++
	13-93B3Cu	5	3	2/3	++/+++

* Key to qualitative assessment of halo density:

0 No halo observed
+ Minor redness surrounding glass bead
++ Complete halo surrounding glass bead
+++ Intense halo surrounding bead

Table III. Quantitative histomorphometric comparison of microvessel densities in tissues at three weeks post implantation. Vessel density values are expressed as area percentage of total tissue observed in the 20x field. Each vessel density value is a mean ± SEM for five replicate tissue samples.

Form of implant	Treatment glass	Vessel area % of 20x field	Fold change relative to sham control
Glass bead	None (sham control)	2.6 ± 0.1	1.0
	13-93	3.5 ± 0.4	1.3
	13-93B3	4.2 ± 0.3	1.6
	13-93B3Cu	6.4 ± 0.9 **	2.5
Microfiber plug	None (sham control)	2.6 ± 0.3	1.0
	45S5	4.1 ± 0.1	1.6
	13-93B3	5.9 ± 0.8 *	2.3
	13-93B3Cu	7.1 ±1.4 **	2.7

* Group mean significantly different from sham control at the $p < 0.10$ level
** Group mean significantly different from sham control at the $p < 0.05$ level

Table IV. Quantitative PCR measurements of cytokine gene expression in skin tissues with sham or borate bead implants. The ΔCt values represent differences between target gene and endogenous control gene expression; each ΔCt value is a mean ± SEM for three replicate tissue samples. The ΔΔCt values represent fold changes of target gene expression relative to a sham control.

Target gene	Bead type implanted	Implant duration (weeks)	Mean ΔCt n=3	Mean ΔΔCt value
FGF2	none (Sham)	2	8.4 ± 0.3	1.00
	13-93B3Cu	1	9.3 ± 0.3	0.53
	13-93B3Cu	2	8.5 ± 0.3	0.81
	13-93B3Cu	3	8.4 ± 0.3	0.93
VEGF	none (Sham)	2	4.8 ± 0.2	1.00
	13-93B3Cu	1	5.2 ± 0.2	0.78
	13-93B3Cu	2	4.7 ± 0.1	1.12
	13-93B3Cu	3	4.0 ± 0.3*	1.80

* Group mean significantly different from sham control at $p < 0.10$

It is helpful to note that ΔCt is inversely proportional to amount of target gene mRNA present in the sample extract.

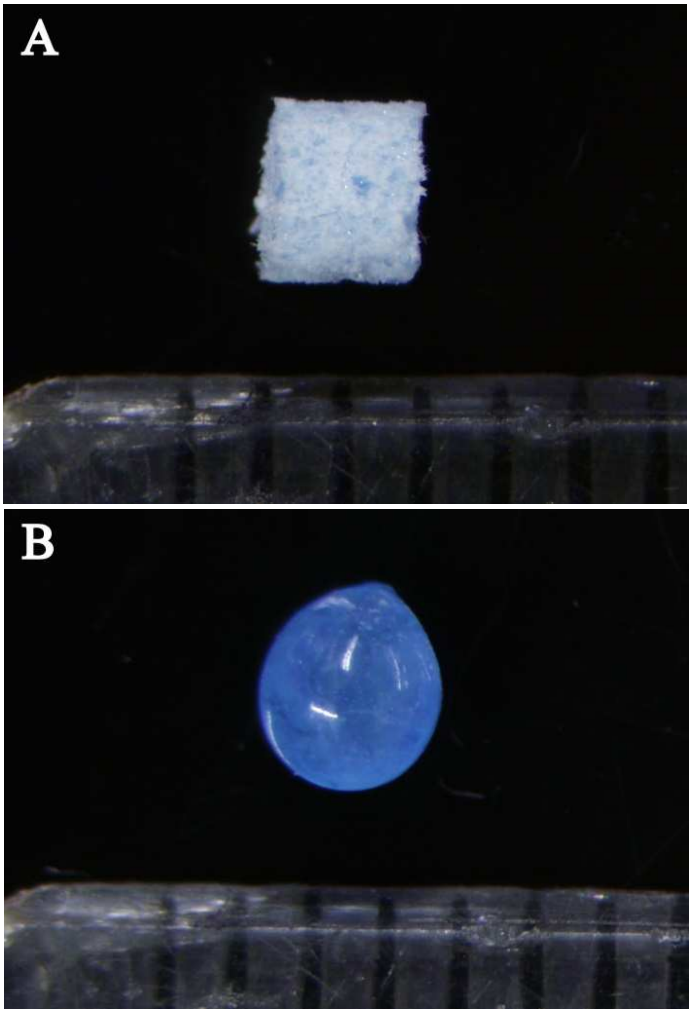

Figure 1. Two separate physical forms of the bioactive glass samples implanted in mice. (A) Compressed 2 mm diameter plugs of glass microfibers (side view); (B) fused 2 mm diameter glass bead. Both samples shown here are 13-93B3Cu glass.

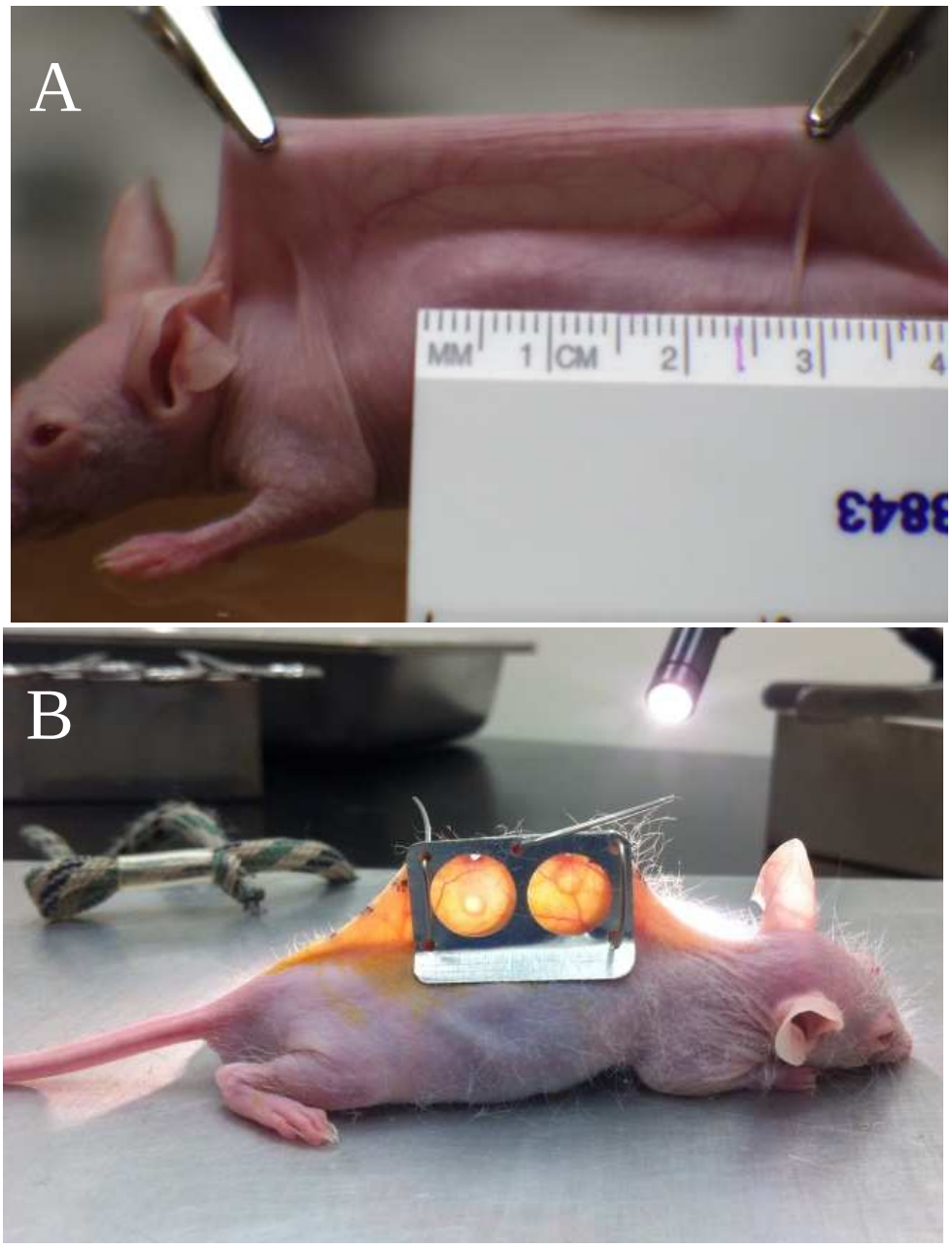

Figure 2. Lifting of dorsal skin fold and installation of skin window frame in SKH1 hairless mice. (A) viewing major transverse vessels in skin fold; (B) mouse immediately after surgical implantation of beads and attachment of skin window frame.

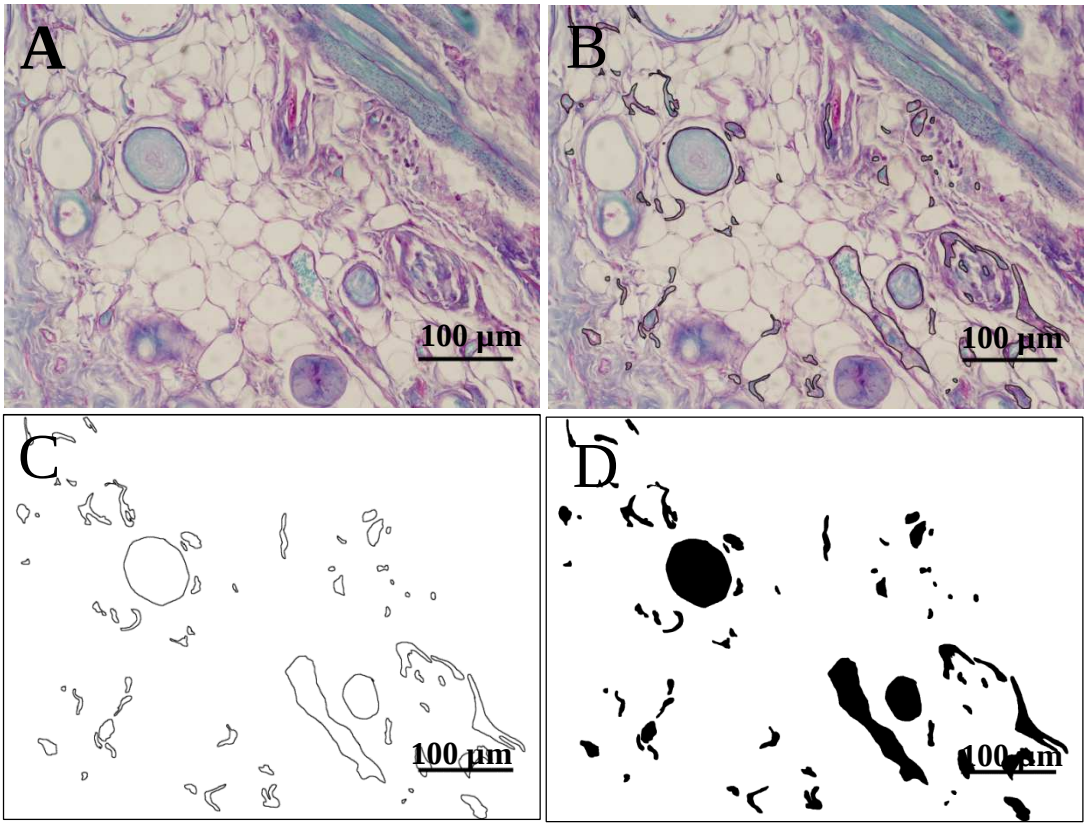

Figure 3. Steps of image processing for histomorphometry of microvascular density in soft tissues. (A) Original color photomicrograph of PAS-stained tissue; (B) Visible blood vessels encircled; (C) Image converted to 16-bit, and the threshold adjusted to highlight encircled area, and image converted to binary. (D) Encircled areas filled with black and filled area measured with ImageJ software.

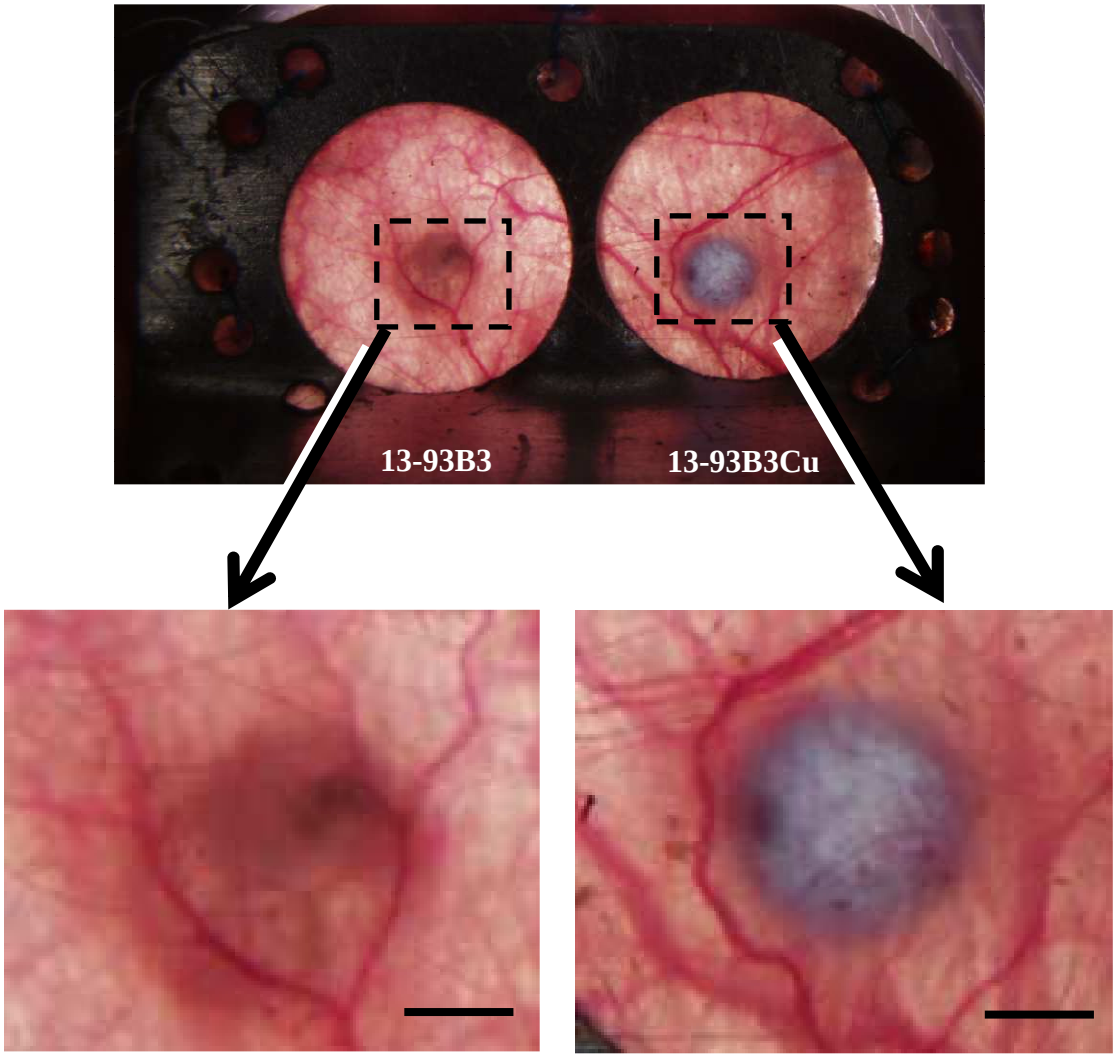

Figure 4: Representative live photo image of localized tissue response to bioactive beads at 1 week post-implantation. Enlarged areas show only little or no halo response around the implanted beads. Scale bars represent 1.0 mm.

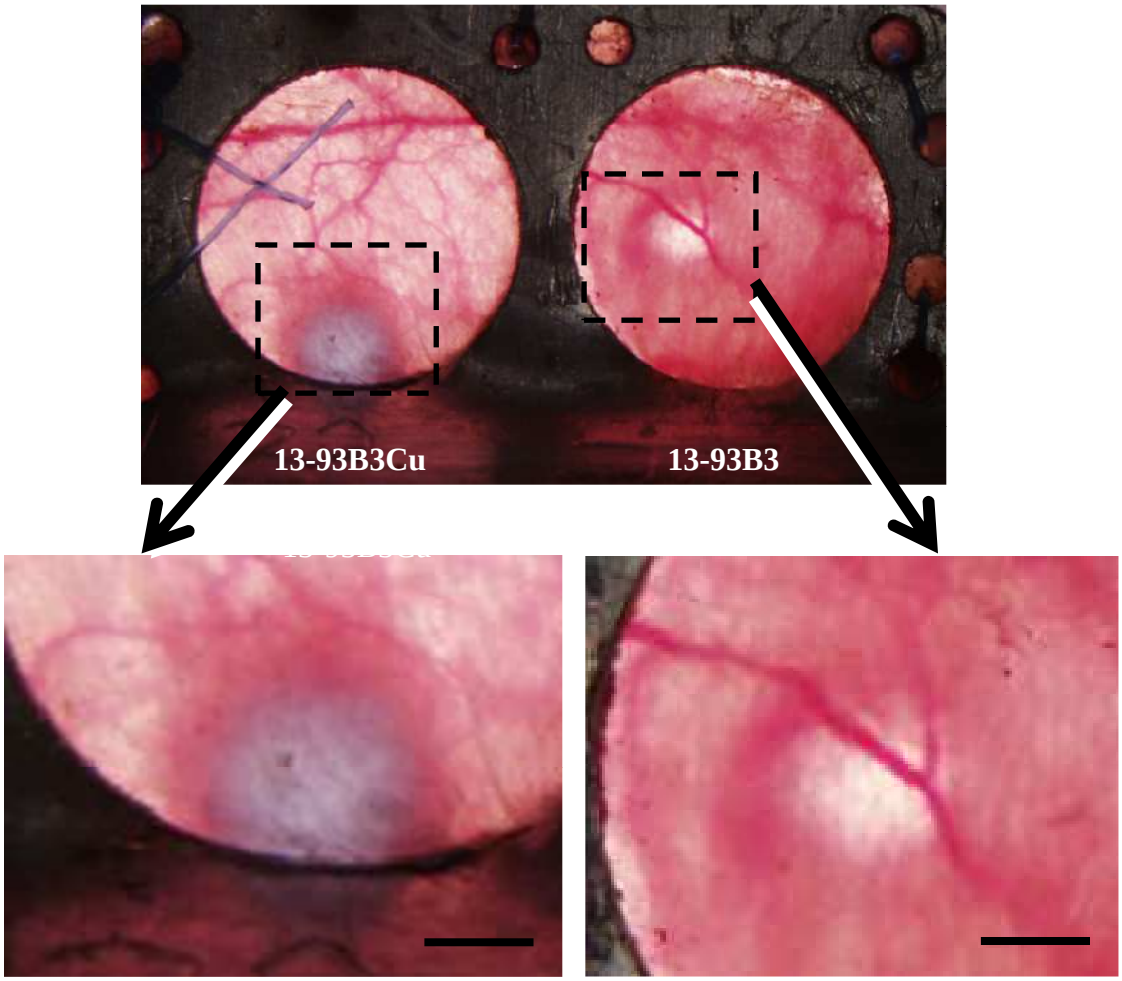

Figure 5: Representative live photo image of localized tissue response to bioactive beads at 2 weeks post-implantation. Enlarged areas show a prominent halo-like structure surrounding the 13-93B3Cu bead. Scale bar represents 1.0 mm.

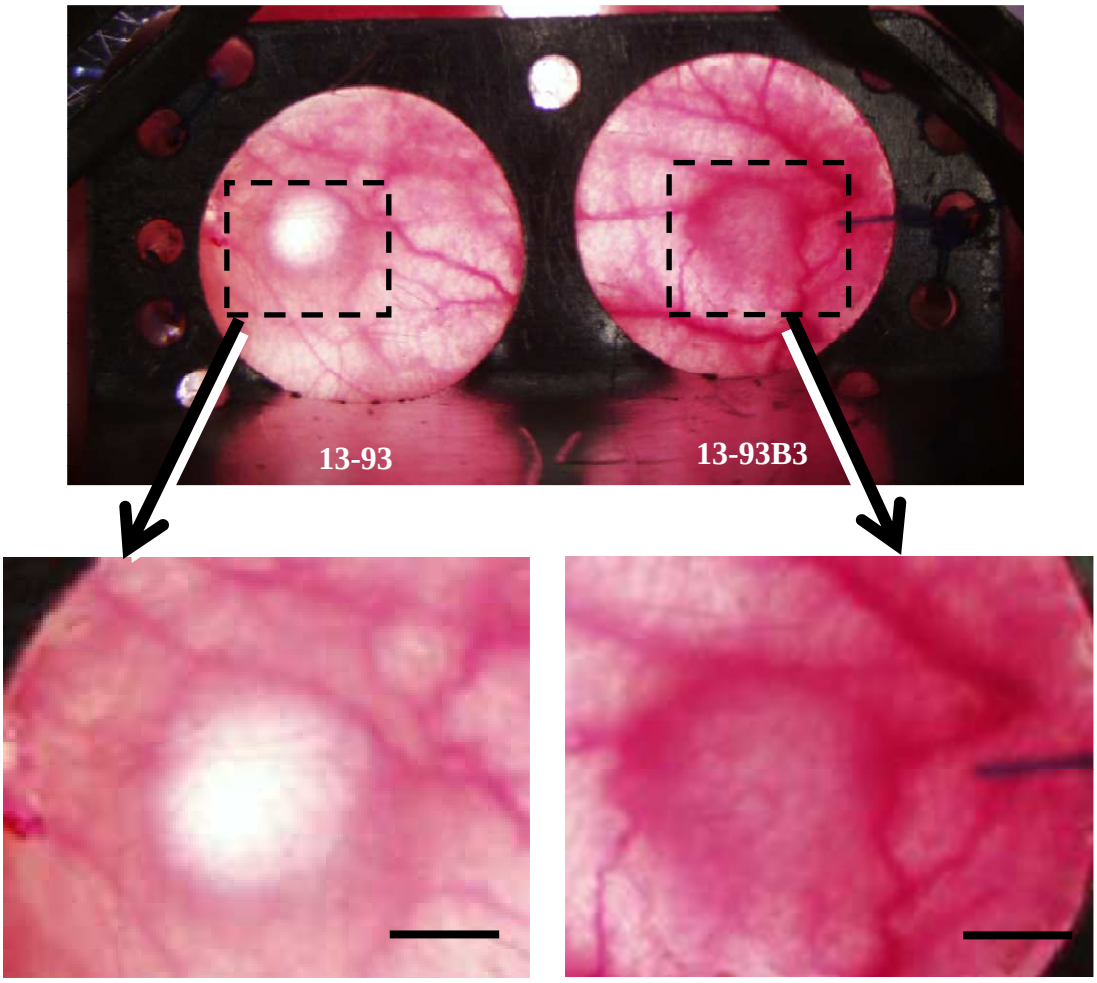

Figure 6: Representative live photo image of localized tissue response to bioactive beads at 3 weeks post-implantation. Enlarged areas show prominent halo around the borate bead; none around the silicate bead. Scale bar represents 1.0 mm.

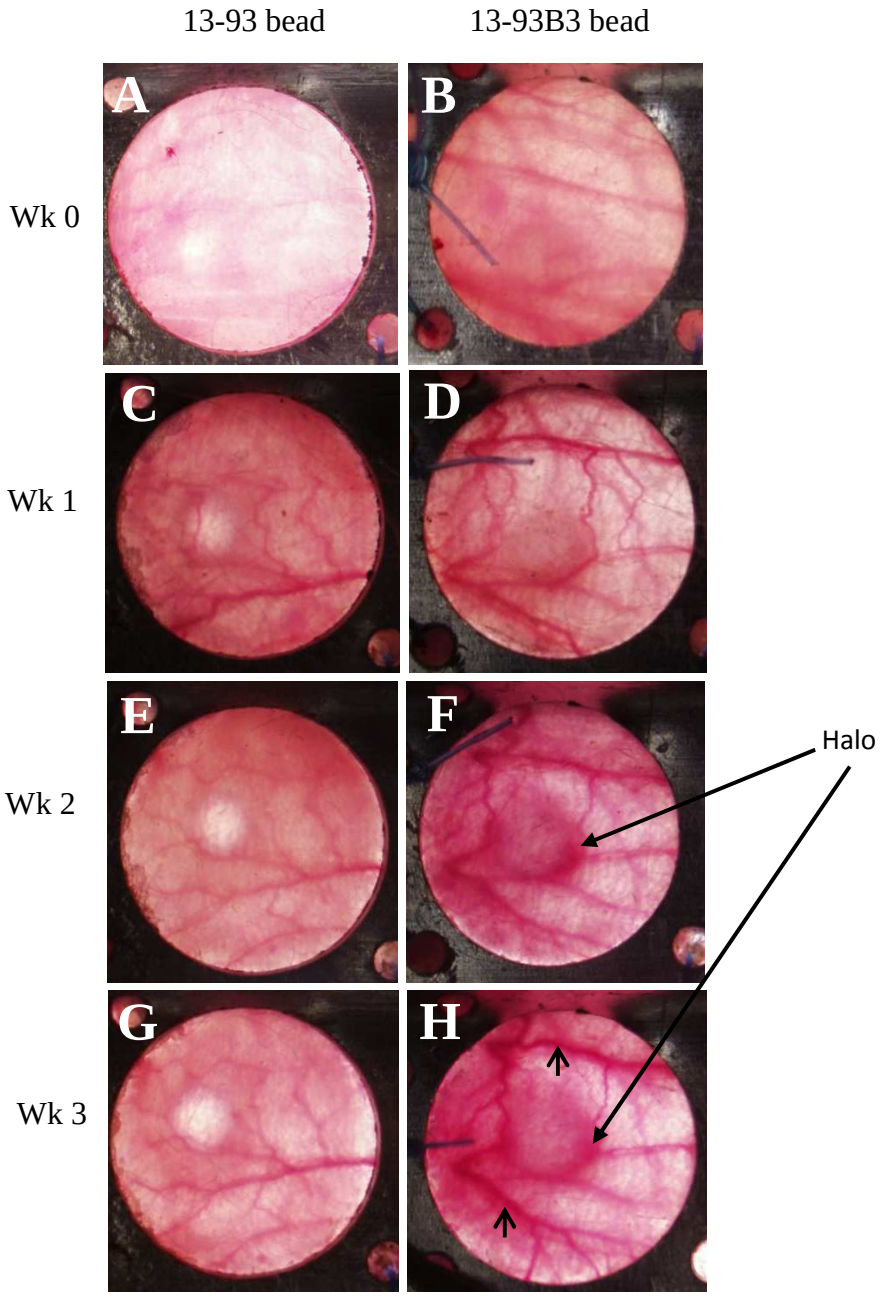

Figure 7. Comparison of three week progression of tissue responses to implantation of 13-93 bead and 13-93B3 bead. Arrows denote halo-like structure around 13-93B3 bead that became prominent at two weeks. Arrowheads point to increasingly prominent larger vessels.

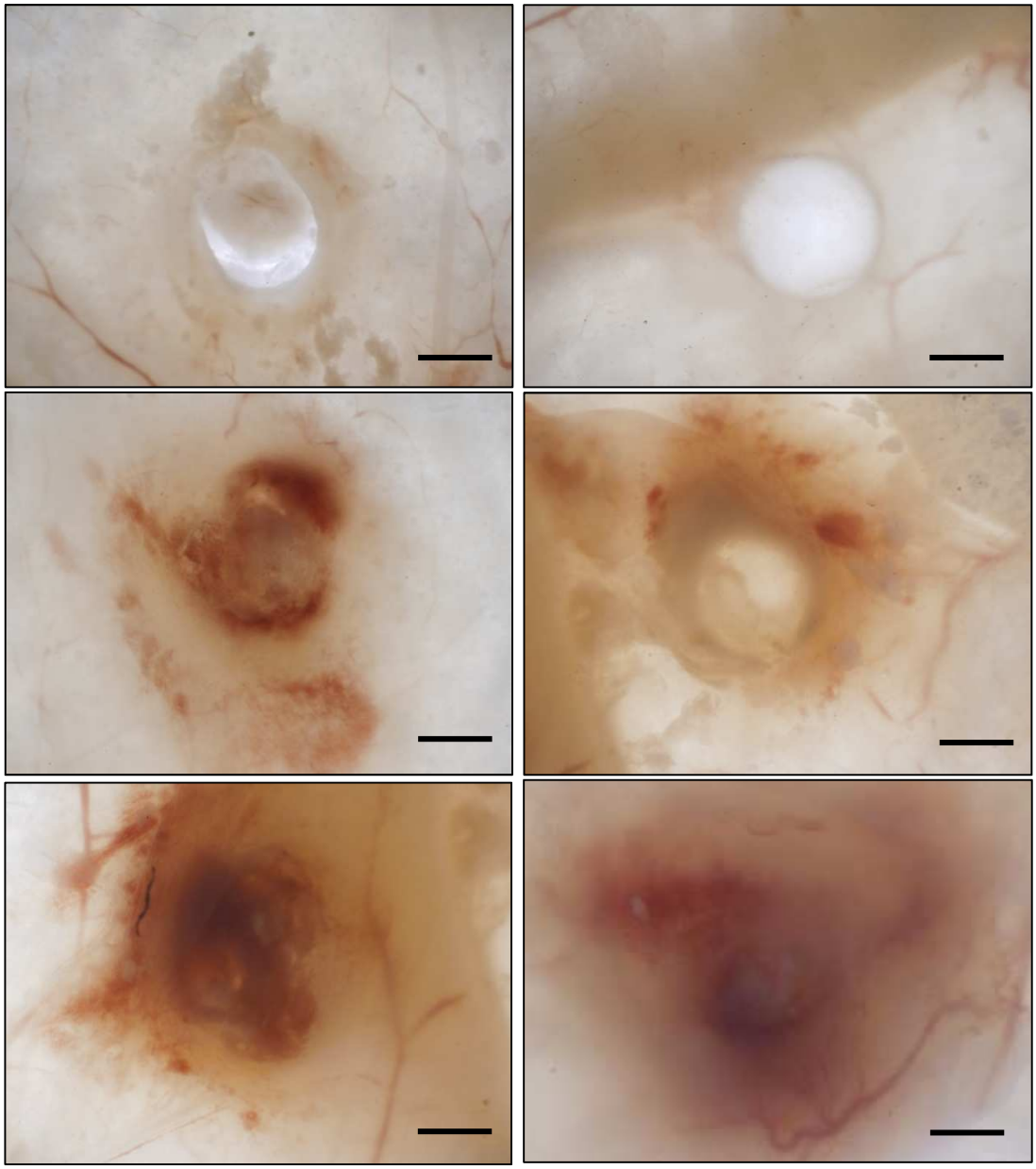

Figure 8. Representative 3 week photo images of beads implanted subdermally without skin window frames. Beads were photographed from the subdermal side rather than by indirect viewing through the skin from the epidermal side. The types of glass beads implanted were: (A-B) 13-93; (C-D) 13-93B3; and (E-F) 13-93B3Cu. Scale bar represents 1 mm.

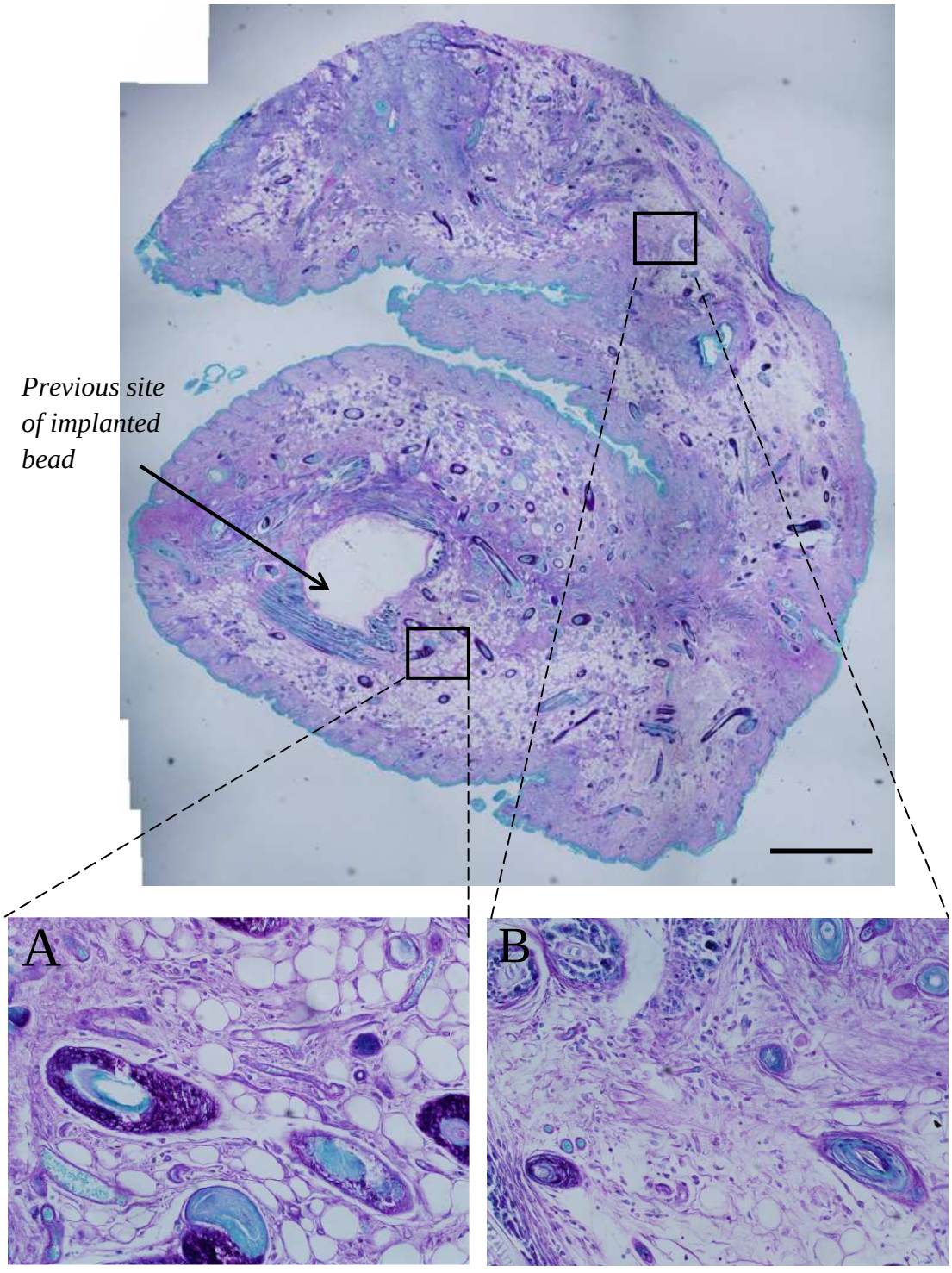

Figure 9. Composite images of soft tissue from a dorsal skin fold implanted with 13-93B3Cu bead. Enlarged area shows relative density of microvessels three weeks post implantation at periphery (A) and near the implanted bead (B). Scale bar represents 1.0 mm.

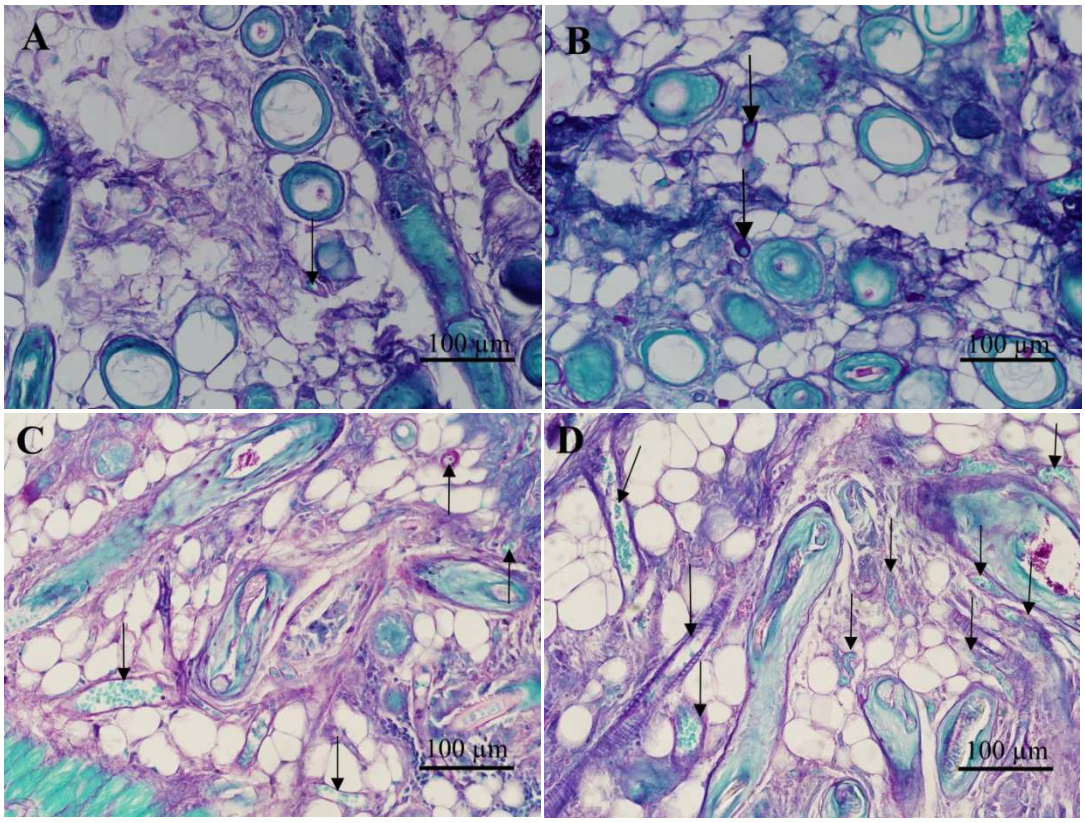

Figure 10. Representative 20x photo images of PAS-stained sections of tissue recovered after 3 weeks from subcutaneous sites of implantation of fused bioactive glass beads. The types of glass beads implanted were: (A) none (sham control); (B) 1393 glass; (C) 13-93B3 glass; and (D) 13-93B3Cu. Arrows point to some of the microvessels seen in the tissues.

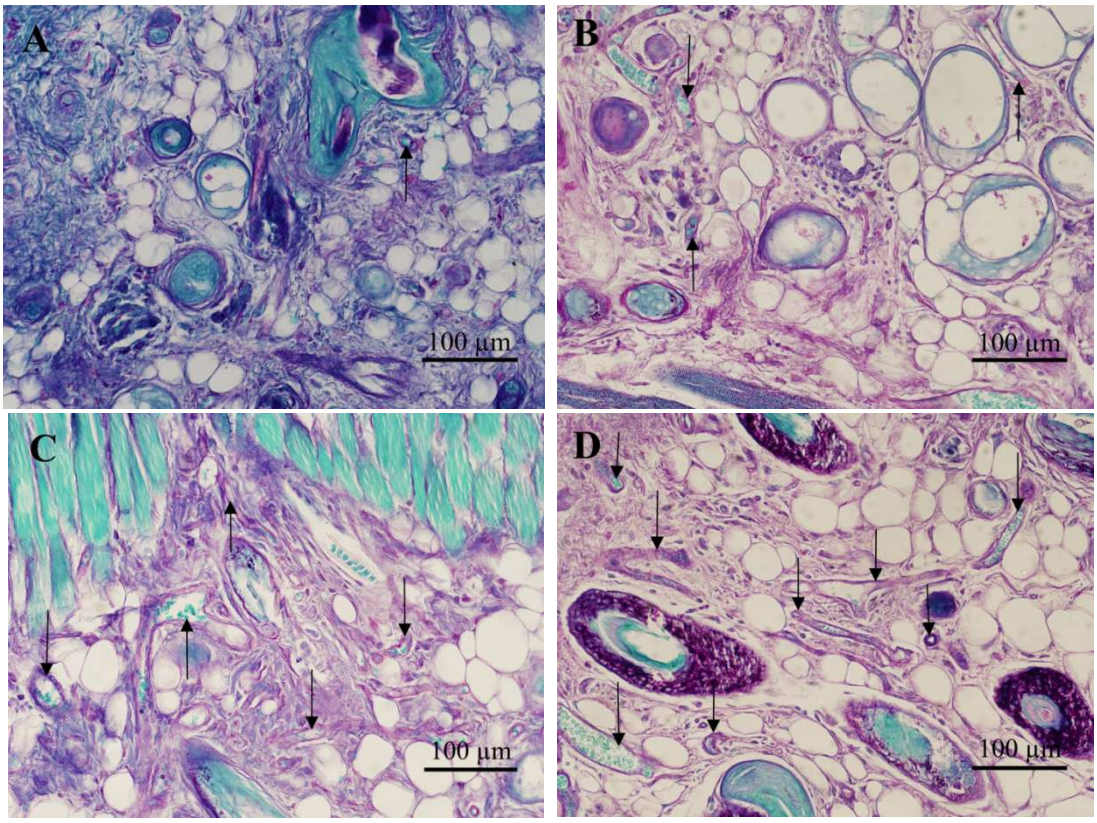

Figure 11. Representative 20x photo images of PAS-stained sections of tissue recovered after 3 weeks from subcutaneous sites of implantation of bioactive glass microfibers. The types of microfibers implanted were: (A) none (sham control); (B) 45S5 (C) 13-93B3; and (D) 13-93B3Cu. Arrows point to some of the microvessels seen in the tissues.

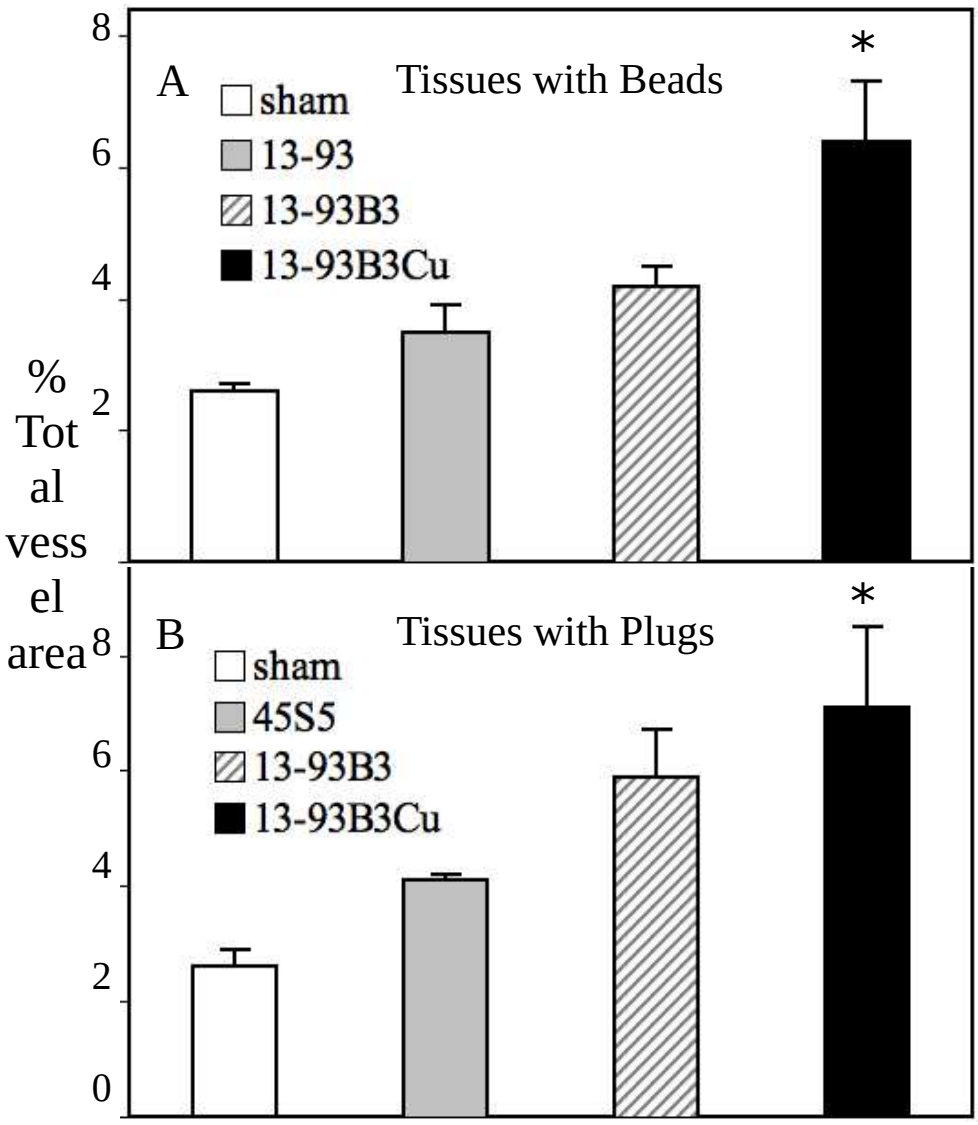

Figure 12. Statistical comparison of vessel densities three weeks post implantation in response to (A) fused bioactive glass beads and (B) microfibrous plugs. Values are means ± SEM for five replicates with each material. Asterisks (*) identify group means significantly different from sham control at $p < 0.05$.

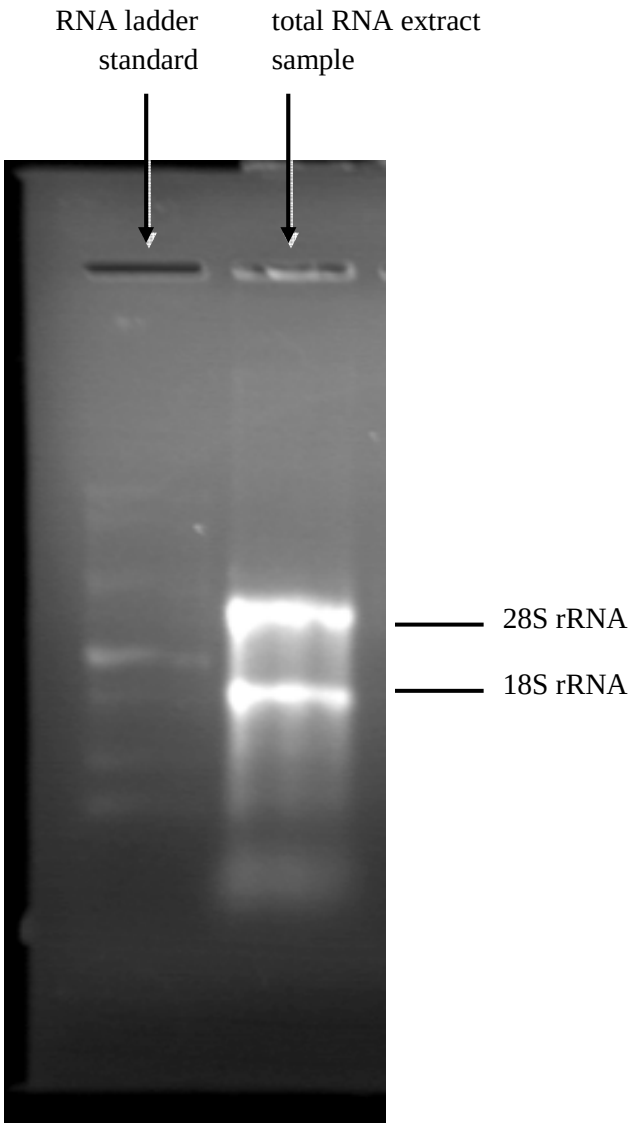

Figure 13. Comparison of agarose gel banding patterns of a sample RNA extract and a ladder standard. Bright bands in gel lane with extract denote positions of 28S and 18S ribosomal RNA.

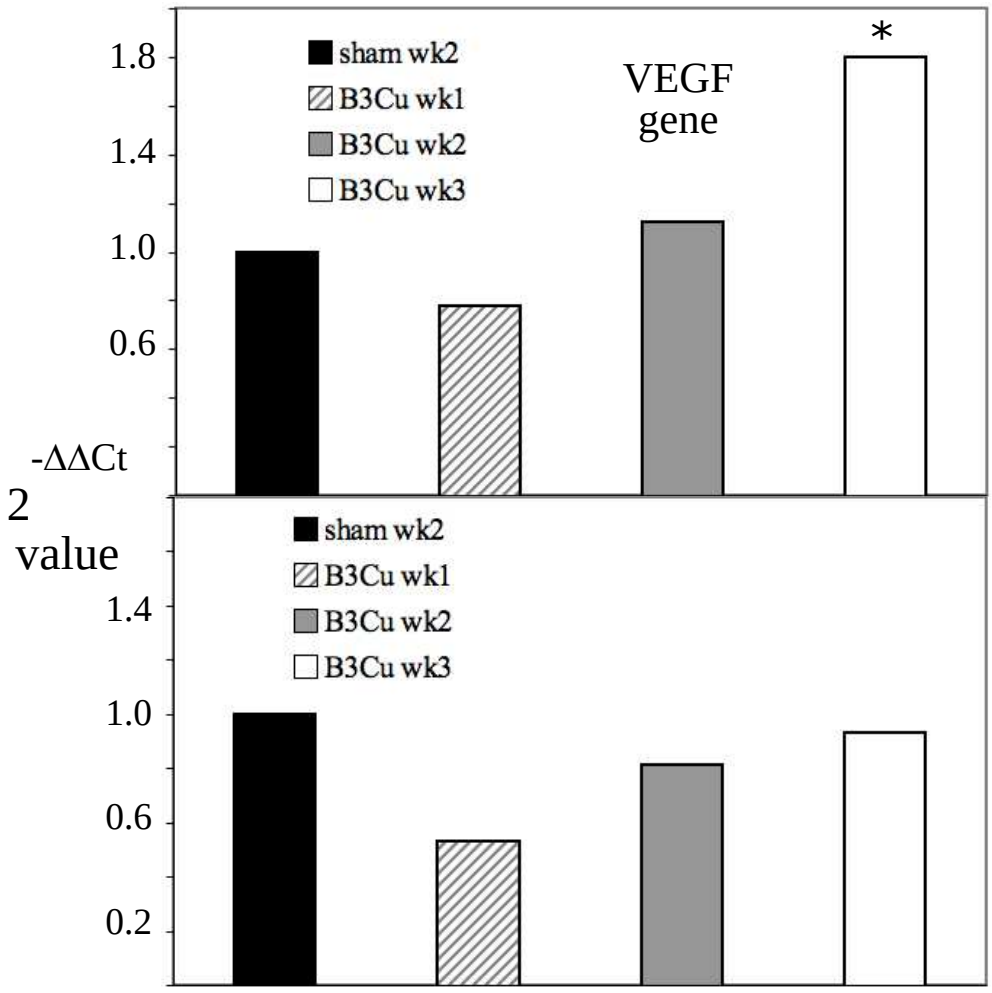

Figure 14. Relative quantitation of FGF-2 and VEGF target genes using the delta-delta Ct calculation. Values are for three replicate with each implant duration. Asterisks (*) identify group means significantly different from sham control at $p < 0.10$

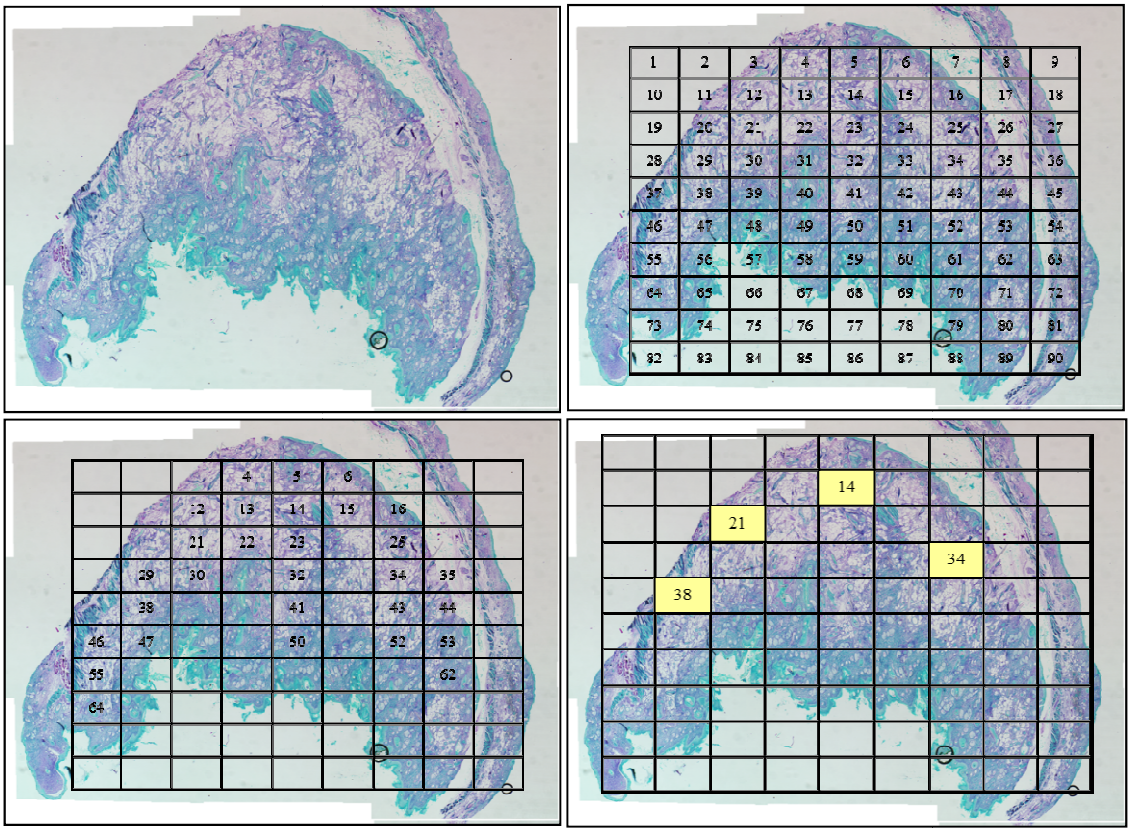

Figure 15. Steps of randomly selecting 20x fields for quantification. (A) Composite image of PAS-stained tissue; (B) Grid overlay scaled such that each box represents a 20x field; (C) Array of qualifying candidate subdermal field for quantification; (D) Four selected subdermal fields to be assessed.

VITA

Richard Jeffrey Watters was born in McAlester, Oklahoma to Christopher and Lori Watters. He graduated from Vicenza High School in Vicenza, Italy in 2004. He graduated from Missouri University of Science and Technology in the Fall of 2011 with a B.S. in Biological Sciences. In the Spring of 2012 he began his graduate degree under Dr. Roger Brown at Missouri University of Science and Technology in the Spring of 2012. He received his Master of Science degree from Missouri University of Science and Technology in May 2014.